UC Berkeley
UC Berkeley Electronic Theses and Dissertations

Title

Electrostatically Charged Polymers for Energy Harvesting and Air Filtration Applications

Permalink

https://escholarship.org/uc/item/68b2m5t0

Author

Ramirez, Neil Stanley

Publication Date

2022

Peer reviewed|Thesis/dissertation

eScholarship.org Powered by the California Digital Library
University of California

Electrostatically Charged Polymers for Energy Harvesting and Air Filtration Applications

By

Neil Ramirez

A dissertation submitted in partial satisfaction of the

requirements for the degree of

Doctor of Philosophy

in

Mechanical Engineering

in the

Graduate Division

of the

University of California, Berkeley

Committee in charge:

Professor Liwei Lin, Chair
Professor Ana Arias
Professor Lisa Pruitt

Fall 2022

© Copyright 2022
Neil Ramirez
All rights reserved

To Britney and Kwan for the support.

Abstract

Electrostatically Charged Polymers for Energy Harvesting and Air Filtration Applications

by

Neil Ramirez

Doctor of Philosophy in Mechanical Engineering

University of California, Berkeley

Professor Liwei Lin, Chair

Polymers are primarily known as insulators with low electrical conductance which make them potentially good candidates as electret materials to store high surface charges for various applications. This work focuses on the investigations of electrostatic charging process and the capability of electret polymers for two specific applications in energy harvesting and air filtration systems.

An energy harvester can use polymeric electret materials in the form of a parallel-plat capacitor to convert mechanical deformations to electrical energy outputs. A prototype piezoelectret device made of FEP (fluorinated ethylene propylene) as the top and bottom electret layers, PET (polyethylene terephthalate) as the middle layer, and EVA (ethylene-vinyl acetate) as the adhesion layer at the boundary has been proposed and demonstrated. A device of 3 cm x 2 cm in size shows a peak output voltage of 8 Volts and 2 μA under the manual compression condition. By using the standard 40 kHz ultrasonic excitation in a beaker under the water environment, a voltage output of 7 Volts has been generated, which is used in the electrolysis process to generate hydrogen at a measured rate of 0.217 ppm/min.

A second piezoelectret energy harvester is proposed and constructed based on biodegradable materials. The device consists of cellulose as the structural supporting layer, PLA (polylactic acid) as the electret, and PEDOT: PSS (poly(3,4-ethylenedioxythiophene) polystyrene sulfonate) as the conductive electrode. Experimental results show the device can generate an output peak-to-peal voltage of 12 Volts under pressure applied by a human hand and hold an initial surface charge of 148 Volts. Preliminary studies have also been performed on silicon dioxide, which has the highest reported surface charge density at the level of 3400 nC/cm^2, about 1~2 orders of magnitude higher than those of polymer materials. However, the high residual stress issue causes the sever defects of the SiO_2 films.

In the third study, polymeric electret materials are investigated for applications in air filtration systems. Several commercial filters are tested for their surface charge potential and longevity. Results show surface potentials in the ambient environment as high as 125 Volts can be maintained over a month-long period. By conducting a new Corona charging process, surface potential as high as 1000V can be achieved for the potential attraction and stiction of harmful viruses and the UV light is proposed as the follow-up process to destruct viruses for applications such as to prevent the spread of COVID-19.

Table of contents

Abstract 1
Table of contents i
List of figures iii
List of tables vii
Acknowledgments viii
1 Introduction and Background 9
1.1 Electrostatic Polymers 9
1.2 Applications and Properties of Electrostatic Polymers 11
1.3 Recent Advances in the State of the Art 14
1.4 Mathematical Framework 16
1.5 Dissertation Outline 18
2 Electrostatic Polymer for Energy Harvesters 20
2.1 Introduction 20
2.1.1 Hydrogen as a Fuel Source 20
2.1.2 Water Splitting and Energy Harvesting 20
2.2 Device Fabrication 21
2.2.1 Fabrication 21
2.2.2 Device Geometry and Working Principle 22
2.3 Results and Discussion 23
2.3.1 Voltage and Current Characteristics 23
2.3.2 Ultrasonication Voltage 25
2.3.3 Surface Charge Potential 26
2.3.4 Gas Generation Quantification 26
2.4 Conclusions 27
3 Biodegradable and Ceramic Piezoelectrets 29
3.1 Introduction 29
3.2 Biodegradable Device 29
3.3 Manufacturing 30

3.4 Prototype Device Fabrication and Testing Results 32
3.5 Biodegradable Device Future Work 33
3.6 Ceramic Piezoelectret 34
3.7 Fabrication and Characterization 35
3.8 Ceramic Device Conclusions and Future Work 36
4 Electrostatic Polymers for Air Filtration 37
4.1 Introduction 37
4.1.1 Air Filtration and Electrostatic Polymers 37
4.2 Evaluation of Electrostatic Characteristics in Commercial Air Filters 38
4.2.1 Commercial Air Filters and Surface Charge Potential 38
4.2.2 One-Minute and One-Hour Corona Charging Study 40
4.2.3 Further 3M6 Material Studies 41
4.3 Case Study: A Generic Air Filter 44
4.4 Air Filtration Conclusions 47
5 Conclusions and Future Work 48
5.1 Electrostatic Polymers for Energy Harvesters 48
5.2 Electrostatic polymers for air filtration 48
5.3 Future Work 48
Bibliography 50

List of figures

Figure 1, Physical deformation of the system. I: Initial system. II: System is compressed and dipole forces from the polymer layers cause the ejection of metal charges. III: System is near maximum compression and a maximum number of metal charge carriers are ejected. IV: System is released from compression state and metal charges build up again. [8]..... 10

Figure 2, The Corona charging process. The polymer plane is grounded and a high voltage is applied between the top needle point and the bottom electrode. The high voltage causes the ionization of air in the ionization region. The electrical field causes ions to drift, which forms the drift region. The dotted lines represent the electrostatic field and the ion flow. In general, the charge density decreases as R increases. [9]..... 11

Figure 3, Ashby Chart of Materials. The materials used for piezoelectret are concentrated in the bottom left corner of the chart. This area represents materials with low densities, leading to light-weight devices. The low Young's Modulus allows superior flexibility compared to ceramics on the top part of the chart. [24] 13

Figure 4, Examples of Piezoelectret Systems. (a)The Finger Driven Nanogenerator is a device made of various layers of materials which generate and collect charge when compressed. Placing one of these devices under a keyboard would allow power generation to occur passively. [22](b)The Human Pulse Sensor is another stacked device that is applied to reading human pulse on the wrist. Traditional Chinese Medicine relies on the pulse at the writs to diagnose various body conditions. This device is an attempt to standardize the practice.[28] (c)The Flowing Kinetic Energy Harvester uses its rotator driven by fluids to generate charges. Like rotors and stators in hydroelectric dams, this device could collect kinetic energy from flowing water to generate electricity. [31](d) The Air Flow Harvester uses the motion of the cantilever to generate charges which can be used to power external devices. Just as a wind turbine uses wind to generate electricity, the airflow harvester could use the displacement of its cantilever to generate energy for an external device.[30] [22], [28], [30], [31] 14

Figure 5, Temperature stable piezoelectret device by a stack of olefin copolymer and PP. The ridges in the COC layer increase the surface area of the charge storage layer which also increases the amount of charge that can be stored. [32]..... 15

Figure 6, Pyroelectric based device by using the PDMS layer with many air voids (white color). These voids can be ionized which leads to a large number of stored charges. The electrodes can collect the charges generated in the polymer layer.[33]..... 15

Figure 7, The device is made of a FEP charge storage layer and Cu/Ag electrodes for charge collection. (a) the device configuration. (b) an array of the device which can

be used to increase the amount of energy generated for the intended application. [34] 16

Figure 8, Capacitive Structure of Piezoelectret. The distance between the top and bottom polymer layers is d. (a) When the top and bottom are far from each other, the distance is d_1.(b) When the device is compressed, and the two polymer layers are near contact, the distance is d_2. [8] 17

Figure 9, (a) Au/PET/EVA/FEP device used for energy generations. (b) Paper/PLA/PEDOT:PSS prototype device for biodegradable energy harvesting applications. (c) Material breakdown of a commercially available air filter for evaluation of its electrostatic properties 18

Figure 10, Energy Harvesting Principle of this work. In the far left an array of piezoelectret devices are disturbed by vibrational energy in the ocean. Middle image shows that this vibrational disturbance causes charge generation on the surface of the devices. The charges start the electrolysis process and hydrogen is released. The far-right figure is the experimental setup image of this concept. 20

Figure 11, Device Fabrication and Geometry. (a) The device is made by creating a stack of materials. The stack is compressed on a hot plate. The heat seals the EVA layers together. (b) The device is charged using the corona charging process. A 15kV voltage is applied to the device which ionized voids within the charge storage layers. (c) The device is covered with Au using a sputtering process for the Au electrode to collect charges. (d) 3D computer rendering. (e) SEM image of the device for the cross section (A-A). (f) PET SEM image, (g) FEP SEM image 22

Figure 12, Device Working Principle. I: device at rest. II: device is compressed, and polymer dipole forces cause charges in the metal layer to release. III: maximum compression occurs, and no more charge can be released. IV: Device is released from compression and charges re-accumulate on the metal layer. 23

Figure 13, Voltage Characteristics via Manual Pressing. Peaks correspond to a manual compression of the device using a finger. Forward and reverse connection are tested to confirm the system is operating due to the mechanical deformations instead of artifacts. 24

Figure 14, Current Characteristics via Manual Pressing. Peaks correspond to manual compression of the device using a finger. The forward and reverse connection are tested to confirm the system is functional instead of artifacts. 24

Figure 15, Optical Image of a Fabricated Device. The gold layer is opaque and prevents the other polymer layers from being seen. The corners show the PET/EVA in the device. 25

Figure 16, Ultrasonic Voltage Characteristics. The inset shows a narrower time range during the operation. 25

Figure 17, Surface Potential Decay. The surface potential starts at 300V after the initial corona charging process. There is a total decay after 15 days. 26

Figure 18, Biodegradable Polymer System. The PLA layer is biodegradable and filled with voids which can be ionized. The nano-paper is made of cellulose and provides mechanical supports to the device. PEDOT: PSS is a conductive polymer which collects the charges generated by PLA. 29

Figure 19, Cellulose and PLA Process: (a) cellulose powder prior to processing; (b) cellulose in an ultrasonic ice bath which separates the microfibers; (c) a bottle of PLA pellets prior to processing. (d) the photoresist spinner used to create PLA thin films. 30

Figure 20, Cellulose Optical and SEM Images: (a)(b) optical photos of the cellulose films for process (a) and (b), respectively. Process (b) is preferable due to its uniform properties as opposed to the clumping seen in (a). (c)(d) The SEM images showing the difference between the fiber morphologies of the layers. 31

Figure 21, Biodegradable Device Prototype. (a) The prototype is held together using an insulating Kapton tape. The PEDOT:PSS is seen in the black ink. (b) Conceptual drawing of the device. 31

Figure 22, Biodegradable Prototype Response. The peaks correspond to manual compression of the device using a finger. Peak to peak voltage is about 12V which is well over the voltage required to power most small electronics. 32

Figure 23, Biodegradable Substrate Charging. Results show quick surface potential decay which is unfavorable for long term stability of the system. The samples differ in substrates because cellulose must be deposited on a structural layer. Certain substrates allow storing more charges than others. 33

Figure 24, Footstep Powered Lighting. Footsteps along an array of devices cause compression which releases charges from the devices. These charges can be used to light up nearby bulbs. 33

Figure 25, Illustration of Ceramic Piezoelectret. SiO_2 Air can be ionized and charges can be stored on the SiO_2 layer. 35

Figure 27, SEM Image of SiO_2 Layer. Cracks suggest errors in the growth process but can also be used to store charge. 35

Figure 28, PXRD Results for the SiO_2 Film. The peaks correspond to crystallinity in film layers. 36

Figure 29, Air Filtration Schemes. The micron fiber is positively charged in the middle. High to low concentration distribution of particles causes filtration by diffusion. Gravity causes inertial effects which can filter large particles. Electrostatic effects cause attraction to the micron fiber and thus electrostatic filtration. [104] 37

Figure 30, Commercial Filter Options. 3M produces four options for consumers with varying performance ratings. Honeywell provides five options with similar ratings. [111]..... 38

Figure 31, Virgin Material Charge Study. Most material show negligible charge except the 3MK and 3M6. The study lasted a total of twenty-five days. 39

Figure 32, 20kV, 1-Minute, 5 cm in distance Corona Charging Study. Five materials showed significant charging capabilities: 3MXX, 3MXV, 3MK, 3M6, and 3M3. One material, R4, showed negligible difference in charge before and after the charging process. Environmental changes such as humidity can accelerate the decay of charges [113]. 40

Figure 33, 20kV, 1-Hour, and 5 cm distance Corona Charging Study. 3M6 shows superior charge storage as compared to other materials. Environmental factors such as heat and humidity affect the day-to-day variation of charges. 41

Figure 34, 1 kV, 1-Minute Corona Charging Process. Sample s1 shows negligible initial charge potential. Sample s4 shows high initial potential and slight variations after the charging process. 42

Figure 35, 10kV 1 Minute Charge. The large difference between initial and post processing charge suggests desirable electrostatic charging properties. 43

Figure 36, 5 kV, 1-Minute Corona Charging Process with a 5 cm gap distance. 43

Figure 37, 9kV, 1 Minute and 5 cm in distance Charge process. The 9kV charging shows significant charging that is comparable but lower than that of the 10kV result as expected. 44

Figure 38, Tec de Monterrey Prototype. The prototype is housed in an acrylic chamber. The chamber is filled with cigarette smoke to assess the filtering performance of the prototype. [120] 45

Figure 40, Generic Air Filter Materials: (a) purple paper-like filter, (b) white/transparent mesh, (c) black metallic wire, (d) carbon black filter that looks like a sponge. Each material is evaluated for its electrostatic properties. 46

Figure 41, Generic Air Filter Material Charging Results. The black wire and carbon sponge show low surface charge potentials. The purple air filter shows a high surface charge potential at -230 Volts and the white filter net show a electrostatic surface charge potential at -280 Volts..... 47

List of tables

Table 1 Examples of Piezoelectric Materials 12

Table 2 Hydrogen Generation Results 27

Table 3 Generation Comparisons in Literature 27

Table 4 Common Electret Materials and their Charge Density. 34

Acknowledgments

Thank you to Professor Lin for his advising and to the many Lin lab members who supported me during my program. I'm grateful for the way that Professor Lin encouraged me to find my own way in my program. I have learned many things beyond research from him and I'll take those on my life's journey. Among Lin Lab I want to call out Emmeline Kao, Yichuan Wu, and Takeshi Hayazaka. To this day Emmeline is a mentor to me. I look forward to joining her in the ranks of PhD holders working at the intersection of government and corporate interests. Prof. Yichuan and I spent many hours in the lab together. I thank him for his friendship both inside and outside the lab that we have to this day. After Takeshi graduated, I missed having someone to compete with for earliest morning arrival. Takeshi was also kind enough to train me on various equipment and provide feedback on my work. Finally, I want to acknowledge the wonderful community in skating and volleyball that I have created. Thank you, Betta, Cassey, Bao, and Zee. I appreciate the space that you all gave me to share all the lows and highs. I am a better person because of you.

1 Introduction and Background

1.1 Electrostatic Polymers

Polymers are materials made up of chains of molecules [1]. Imagine a chain of paper clips, the individual clips represent the molecule [2]. The chain represents one of the millions of chains that make up the material. The length of the chains and the strength of the bonds between them determine how a polymer behaves. For example, a polymer with very long chains will be very flexible like a rubber band. A polymer with very short chains will break apart when pulled like an eraser. Most polymers are insulators so charges cannot pass through them. A polymer that is completely solid and has no voids has no chance interacting with charges. A polymer with voids can use its insulating properties to trap electrostatic charges [3]. Applying a large voltage to the polymer can ionize the voids. The ionized charges are then locked within the polymer since the insulating properties of the polymer keep them from leaving the system. The trapping of charges allows the once electrically inactive polymers to have electrostatic properties. When the polymer is deformed, the charges move around. This movement creates dipole forces which can alter the electric field around the polymer. The discovery of electrostatic polymers is attributed to G. Sessler [4], who demonstrated the Carnauba wax could be electrically charged and discharged.

Originally, electrostatic applications were limited to metals since they have superior conducive properties [5]. The materials of choice were metals like copper and aluminum for use as conductors. Glass and other ceramics are the choice for displays. Unfortunately, metals are opaque, rigid, and dense so any devices made of them will have the same properties. When a metal device is dropped, it is likely to crack and break and glass has similar problems. Polymers can be transparent, flexible, low density, and light weight [6], [7]. This opens the possibility of devices that can be made [8]. Where a device primary made of metals might fail when it is bent, a polymer device could be bent with little effects on its performance.

The electrostatic polymer is made up of small voids filled with air. When subjected to a high enough voltage, the air is ionized, and charges are stored within the polymer [9]. Since the polymer is typically an insulator, the charges within the polymer cannot exit. If the polymer is combined with a conductor, the charges are accessible. When the polymer is deformed, charges within the voids are displaced to create dipole forces. These dipole forces acting on the conductive cause free charges to exit the conductor. Attaching conductive wires to the conducting layer allows the collection of these charges. The collecting layer can be a metal or a conductive polymer. There are various reported charging processes including using ionic hair dryers and these processes require that a voltage is applied to the system. The voltage creates an electric field and a potential which causes charges to migrate. This work will focus on charging polymers using the corona charging method to be discussed in more detail in a following section.

To use the charges stored in the polymers, the polymer must be physically or electrically disturbed. **Figure 1** shows how the deformation of the device affects the charges on the aluminum layer [10]. When connected to a complete circuit, the charges on the metal layer can be collected. In this case, the polyethylene terephthalate (PET) acts as

an insulator. An air chamber is created by bonding two PET layers using ethylene vinyl acetate (EVA) as an adhesive. This air chamber can then be charged by the corona charging process. The electrical charges are trapped since PET is an insulator. Adding a metal layer made of aluminum completes the process. Charges displaced during a mechanical compression process of the device as shown cause free charges in the aluminum to exit since aluminum is conductive. In **Figure 1**, the initial state of the system is shown in (I). Charges are stored inside the air chamber in the PET layers. When the device is compressed as shown in (II), some charges in the aluminum layer are expelled as the result of the displacement between charges which causes a dipole moment. In state (III) the device is compressed to its maximum state and the maximum dipole moment has expelled most free charges. Releasing the system as in state (IV) causes charges to reaccumulate on the aluminum layer and return to the initial state in (I).

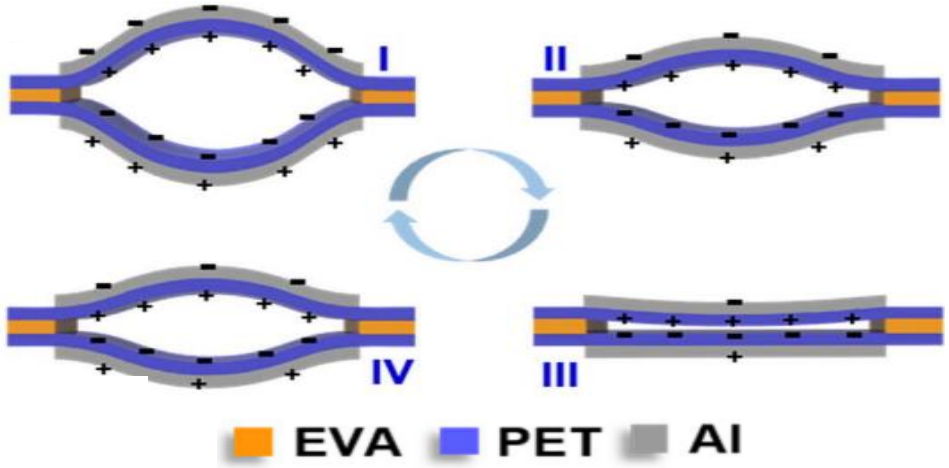


***Figure 1**, Physical deformation of the system. I: Initial system. II: System is compressed and dipole forces from the polymer layers cause the ejection of metal charges. III: System is near maximum compression and a maximum number of metal charge carriers are ejected. IV: System is released from compression state and metal charges build up again.* [8]

Figure 2 is a schematic diagram of the Corona charging process [9]. The polymer (plane) is subjected to a voltage potential by a ground electrode in direct contact with it at the bottom and a sharp electrode tip at the top. The potential is supplied by a high voltage source. The voltage potential must be high enough to break down the air between the polymer and the tip. When this happens, charges are generated in the air and injected onto the polymer material surfaces. The charge collection efficiency can be improved by increasing the temperature of the material and thus increasing the charge mobility. It can also be improved by decreasing the humidity of the system which reduces the dissipation of charges to the environment during charging. Charges will follow the path of least resistance which is why the metal layer must connect electrically to a complete circuit before any charges can be stored. Alternatively charges on the metal layer may be absorbed by environmental ionizers such as moisture and dry air.

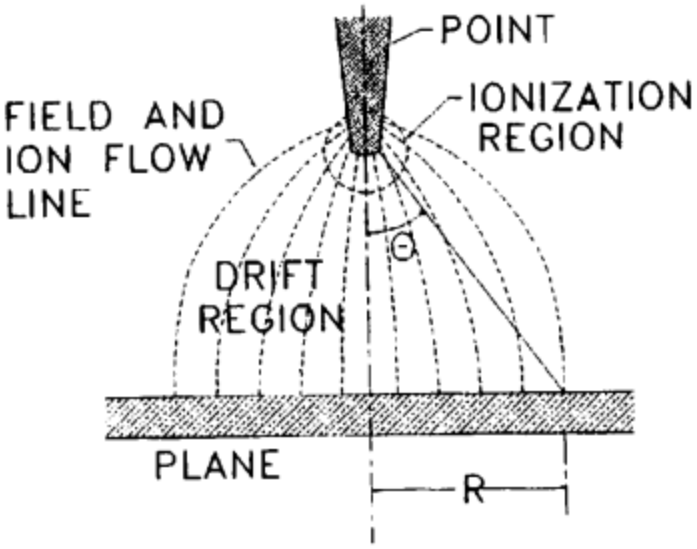


***Figure 2**, The Corona charging process. The polymer plane is grounded and a high voltage is applied between the top needle point and the bottom electrode. The high voltage causes the ionization of air in the ionization region. The electrical field causes ions to drift, which forms the drift region. The dotted lines represent the electrostatic field and the ion flow. In general, the charge density decreases as R increases.* [9]

1.2 Applications and Properties of Electrostatic Polymers

Electrostatic polymers have been used in many engineering applications previously [11]. Given the mechanical to electrical conversion ability of electrostatic polymers, this dissertation primarily focused on applications in energy harvesting and air filtration. In the first application area, energy harvesting is a field of interest due to the longstanding need for power generation in the world [12]. There are various schemes that have been used to collect power from an electrostatic device. In all these schemes, an external circuit is required to access the induced/generated charges. One of the earliest and simplest schemes is to use an electrostatic polymer energy generator which is wired to an LED or LCD to light it up. The electric power is generated from the electrostatic polymer by physically pressing the polymer with a finger or a foot. Other schemes include using wind, wave, and sound disturbances as the energy sources to repeatedly deform the energy generators.

The second application area is the air filtrations. Air purification has been of interest for a long time in many sectors, including industrial environments. This field has caused more attentions in the COVID-19 pandemic due to its airborne spread mechanism. One way to increase the filtration efficiency of collecting viruses/dusks in the air is to electrostatically charge the filters [13]. The charges on a filter can attract and repel charges that make up air pollution or viruses [14]. This creates the possibility for electrostatically charged polymers to be used in the air filtration application [15].

Table 1 shows examples of piezoelectric materials [16], including ceramics such as ZnO, PZT, and WeS_2. These materials are fabricated using high temperature processes. For example, ZnO can be grown using a high temperature oxidation process. Another example is AlN which can be grown using a high temperature chemical vapor deposition process.

Table 1 *Examples of Piezoelectric Materials*

Materials
ZnO
MoS_2
WSe_2
PMN-PZT/PT
PZT
Alkaline Niobate (KNLN)
$BaTiO_3$
AlN
PVDF
Cellular PP
PMDMS
PET/EVA/PET
FEP
M13 bacteriophage
Fish Swim Bladder

Examples of polymers include common polymers such as PVDF (polyvinylidene fluoride), PET, EVA, and FEP (fluorinated ethylene propylene), which are all commonly used in consumer plastic products [8], [17], [18]. PVDF can be used in a variety of industries including food packaging as a chemical resistance material. PET can be found in disposable cups and EVA is a common adhesive. These polymers are generally made by using processes such as chain reaction and condensation. Piezoelectric materials that might surprise some are fish bladders and bacteriophages. In general, if a material has voids that can be filled with charges, it can act as an electret. The most popular materials for electrostatic applications are ZnO [19] and PZT [20]. Although they are subject to brittle failure, their high electrostatic potential breakdown voltages make them the material of choice in many applications. For example, PZT is commonly used in microphone and speaker applications such as in cell phones. Ultimately, one will choose a material based on the desired application. For example, if the final device needs to withstand high temperature operations, ceramic materials are selected due to the excellent stability in high temperature conditions [21]. Applications that require flexibility often use polymers [22], [23]. Overall, the material choice is also limited to processing techniques and the final electrostatic performances.

Figure 3 shows the Ashby Chart [24] with the visual representation of various common materials used in Engineering. The polymer materials used for electrostatic applications are labeled as foams, polymers, and elastomers. Two important material properties are plotted in the figure: density, and Young's Modulus. The density of a material is an important property because it will determine the overall weight of the device for its intended application [25]. The Young's modulus is related to the flexibility of the

material. The use of rigid materials with high modulus in devices can lead to brittle failures such as the crack of phone screen due to high mechanical impacts or other mechanical failures due to high mechanical bending stresses [26]. On the other hand, piezoelectret materials are concentrated in the bottom left corner of the figure. This area represents materials with low densities, leading to light-weight devices and low Young's Modulus, allowing superior flexibility as compared to ceramics on the top part of the chart.

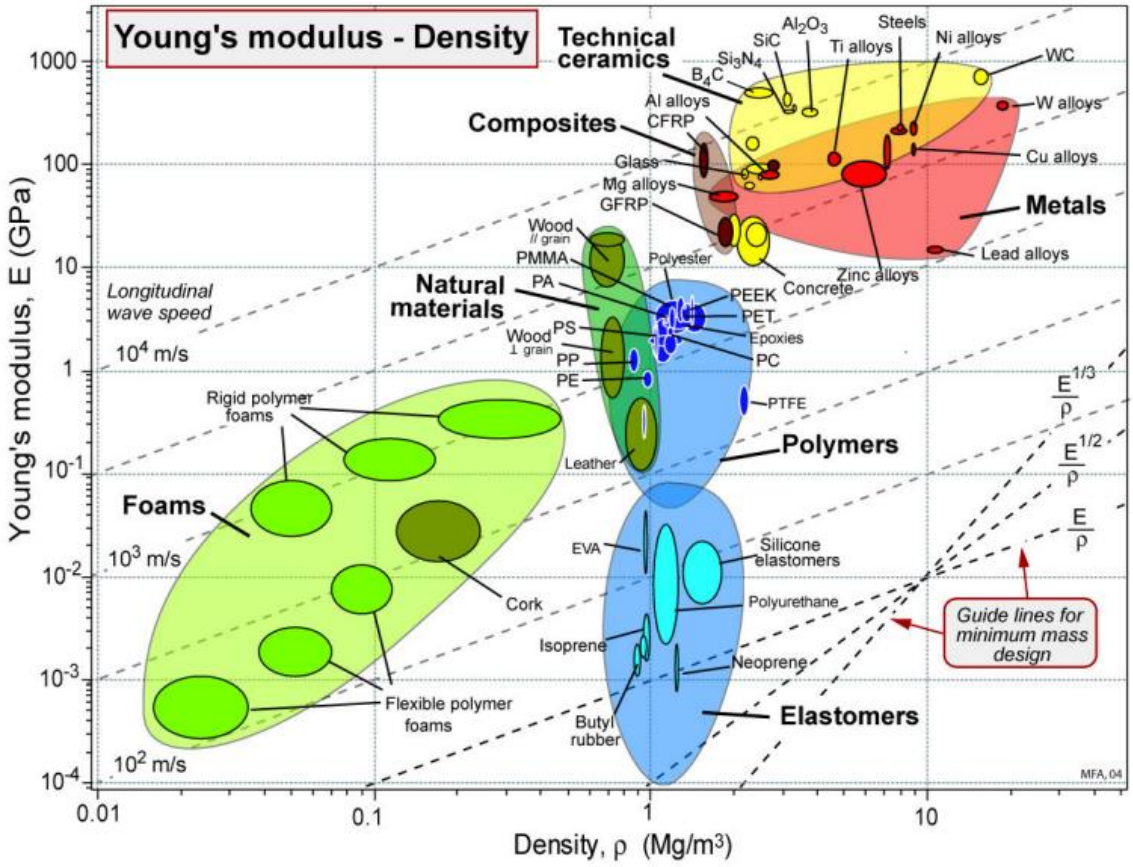


Figure 3, *Ashby Chart of Materials. The materials used for piezoelectret are concentrated in the bottom left corner of the chart. This area represents materials with low densities, leading to light-weight devices. The low Young's Modulus allows superior flexibility compared to ceramics on the top part of the chart.* [24]

Electrostatic polymers have been implemented in a variety of devices [25][26]. **Figure 4** shows four examples. All examples include an electrostatic polymer combined with a metal for charge collection. There are also actuator devices that use the electrical input to cause a mechanical output. These are not discussed in this work. **Figure 4a** is a finger-driven nanogenerator with PFTE and PET electrets to generate energy by using Cu and Ag as charge collectors [27]. In this case, the device can be pressed with a finger to generate electricity to light up external lights. **Figure 4b** shows a human pulse sensor using FEP as the electret material and Au is the charge collecting material. [28]. This device is sensitive enough to turn the mechanical human pulse motion on the wrist as electrical

outputs. **Figure 4c** is the flowing kinetic energy harvester with Fluorine based polymer as the electret material and gold as the electrode [29]. Energy is harvested by the relative mechanical movements between the rotator and stator. **Figure 4d** is the airflow harvester with PFTE as the electret material and Cu is the charge collecting material [30]. The airflow causes the cantilever to deform and the resulting charges can be collected.

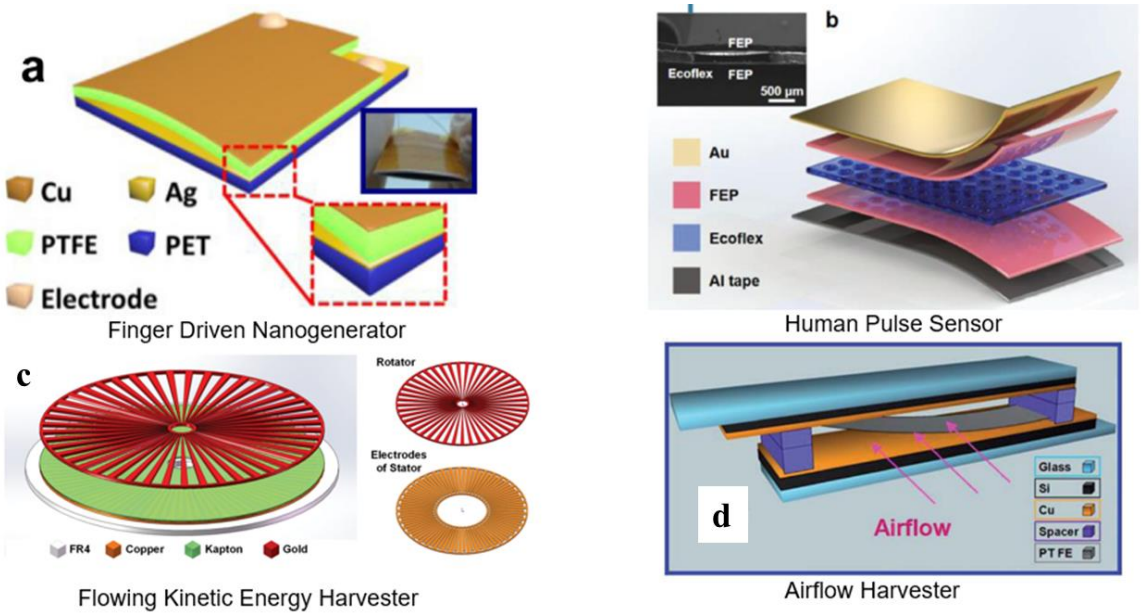


Figure 4*, Examples of Piezoelectret Systems. (a)The Finger Driven Nanogenerator is a device made of various layers of materials which generate and collect charge when compressed. Placing one of these devices under a keyboard would allow power generation to occur passively.* [22]*(b)The Human Pulse Sensor is another stacked device that is applied to reading human pulse on the wrist. Traditional Chinese Medicine relies on the pulse at the writs to diagnose various body conditions. This device is an attempt to standardize the practice.*[28] *(c)The Flowing Kinetic Energy Harvester uses its rotator driven by fluids to generate charges. Like rotors and stators in hydroelectric dams, this device could collect kinetic energy from flowing water to generate electricity.* [31]*(d) The Air Flow Harvester uses the motion of the cantilever to generate charges which can be used to power external devices. Just as a wind turbine uses wind to generate electricity, the airflow harvester could use the displacement of its cantilever to generate energy for an external device.*[30]

1.3 Recent Advances in the State of the Art

Recent advances in the energy harvesting using piezoelectric and electromagnetic technique have been reviewed previously [31]. Here, the schemes on electrostatically charged polymer engineering are discussed in three focuses: environmental stability, charging effectiveness, and system integration. The temperature limitation of polymers is an important factor as polymers either melt or lose their charge storage capabilities subjected to a high temperature. On the other hand, to maximize the efficiency of electrostatically charged polymer, the electrostatic charging effectiveness must be considered in various fabrication processes and applications. Finally, device integration is reviewed for electrostatic polymers and in various applications.

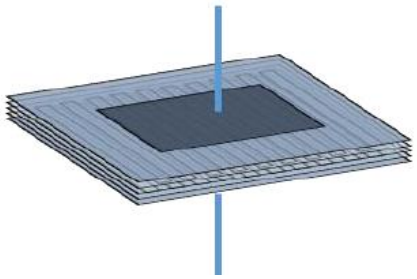


Figure 5, *Temperature stable piezoelectret device by a stack of olefin copolymer and PP. The ridges in the COC layer increase the surface area of the charge storage layer which also increases the amount of charge that can be stored.* [32]

Figure 5 shows a computer model of a piezoelectret device that is capable of withstanding high temperatures. The device is made of a hybrid cyclic olefin copolymer (COC) and polypropylene (PP) [32]. PP acts as the structural layer and the COC is the charge storage layer. After charging the device, it is subjected to 200 hours of annealing at 110 ºC. The report shows that the device can retain 25% of its electrical activity after the annealing process. By comparison, a device with only PP loses all electrical activity after 16 hours of an annealing process at 70 ºC. This results show a promising approach toward devices for high temperature applications.

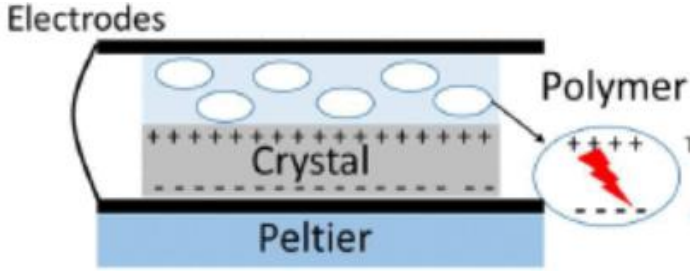


Figure 6*, Pyroelectric based device by using the PDMS layer with many air voids (white color). These voids can be ionized which leads to a large number of stored charges. The electrodes can collect the charges generated in the polymer layer.*[33]

Figure 6 shows a polydimethylsiloxane (PDMS) piezoelectret device that is charged using the pyroelectricity effect. Generally, the corona charging method is energy intensive because it requires a very high voltage to operate and the high energy cost. It is reported that using a process with a temperature gradient from 10-70 ºC at a rate of 2 ºC/s can charge the device [33]. After the charging process, the device demonstrates a peak voltage of 20 mV. While the voltage is much lower than most state-of-the-art piezoelectret devices, the charging method warrants further investigation.

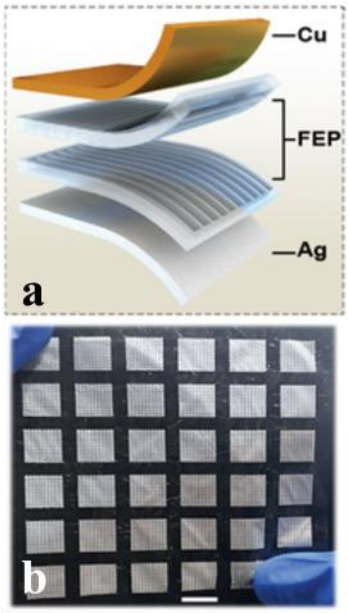


***Figure 7**, The device is made of a FEP charge storage layer and Cu/Ag electrodes for charge collection. (a) the device configuration. (b) an array of the device which can be used to increase the amount of energy generated for the intended application.* [34]

All good piezoelectret systems can use an array design with multiple devices to allow for a greater scope of application. For example, if an application needs to collect energy over an area of 10 m^2, it is impossible in practice for a device to occupy such big area. A possible solution is to stack up many devices in an array. In another example, **Figure 7** shows a computer-generated image of a single device and an optical image of the device array. The device is made of two FEP films with copper and gold electrodes. An array of 5x18 sensors is constructed to measure vascular pulsations. The array sensor design achieves similar accuracy as medical grade pulse sensor systems [34].

1.4 Mathematical Framework

The theoretical framework for piezoelectret has been previously established [35]. The system is modeled as a capacitor with two parallel plate distances of d_1 and d_2 before and after the mechanical compression as shown in **Figure 8**. Compressing the device changes the distance between the capacitor from d_1 to d_2. The following equation shows the capacitance for a parallel-plate capacitor with a plate area A, air permittivity ε_r, and vacuum permittivity ε_0 [36]. The difference between the two capacitors is the distance between plates with either a distance d_1 or d_2.

$$C = \frac{\epsilon_0 \epsilon_r A}{d_1} \tag{1}$$

The work (W) produced by a charge (Q) and capacitance C is derived. in terms of the charge stored, area of the plates, and the permittivity.

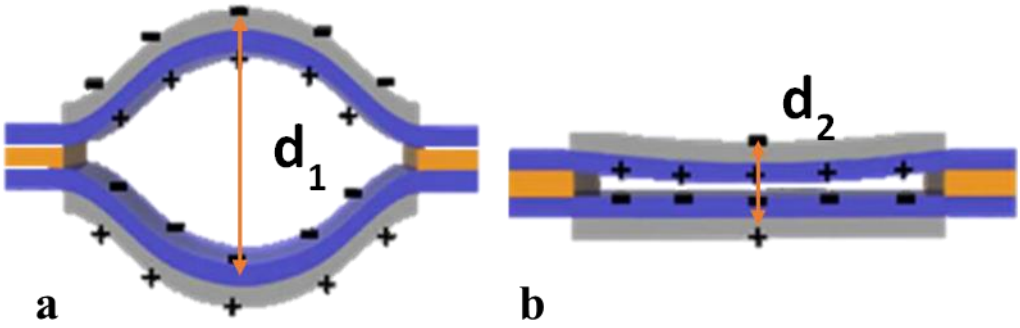


Figure 8, *Capacitive Structure of Piezoelectret. The distance between the top and bottom polymer layers is d. (a) When the top and bottom are far from each other, the distance is* d_1*.(b) When the device is compressed, and the two polymer layers are near contact, the distance is* d_2*.* [8]

$$W = \frac{Q^2}{2C} = \frac{dQ^2}{2\epsilon_0\epsilon_r A} \tag{2}$$

The relationship suggests that the amount of work that the capacitor is capable of producing is directly proportional to the charge to the second power [36]. This means that the charge implanted into the device using the corona charging process is highly indicative of the amount of work that the device can produce. The work is also directly proportional to the distance between the capacitor plates. This means the depth of the voids in the polymers used for this work should be as large as possible. Conversely, increasing the surface area of the device reduces the amount of work that it can produce. The voltage (V) generated by the system is directly proportional to the charged stored in the system Q. The same voltage is inversely proportional to the capacitance of the device.

$$C = \frac{Q}{V} \rightarrow V = \frac{Q}{C} \tag{3}$$

The previous equation is the capacitance expression rearranged to represent the voltage. The voltage generated by a device can be measured directly using a voltmeter. This voltage gives insight to the performance of the device. As a power generator, the device must meet the voltage requirements of the application. For example, to power an LED, the device must generate at least 1.2 V. Re-arranging the equation shows us that reducing the capacitance and maximizing the charge stored in the device will provide the largest voltage. The surface charge is proportional to the voltage generated by the system. Monitoring the surface charge provides an estimate for voltage that a device can generate.

$$\sigma = \frac{Q}{A} \rightarrow \sigma \alpha V \tag{4}$$

The surface charge is the number of charges on the device over a given area. Relating the charge to the voltage shows that the surface charge is proportional to the voltage generated. This means that the voltage, which dictates what kind of devices can be powered, relies directly on the amount of charge the system stores.

1.5 Dissertation Outline

This dissertation focuses on the use of electrostatically charged polymers in energy harvesting and air filtration applications, including the polymer material selection and synthesis, device fabrication, and system characterizations as illustrated in **Figure 9**.

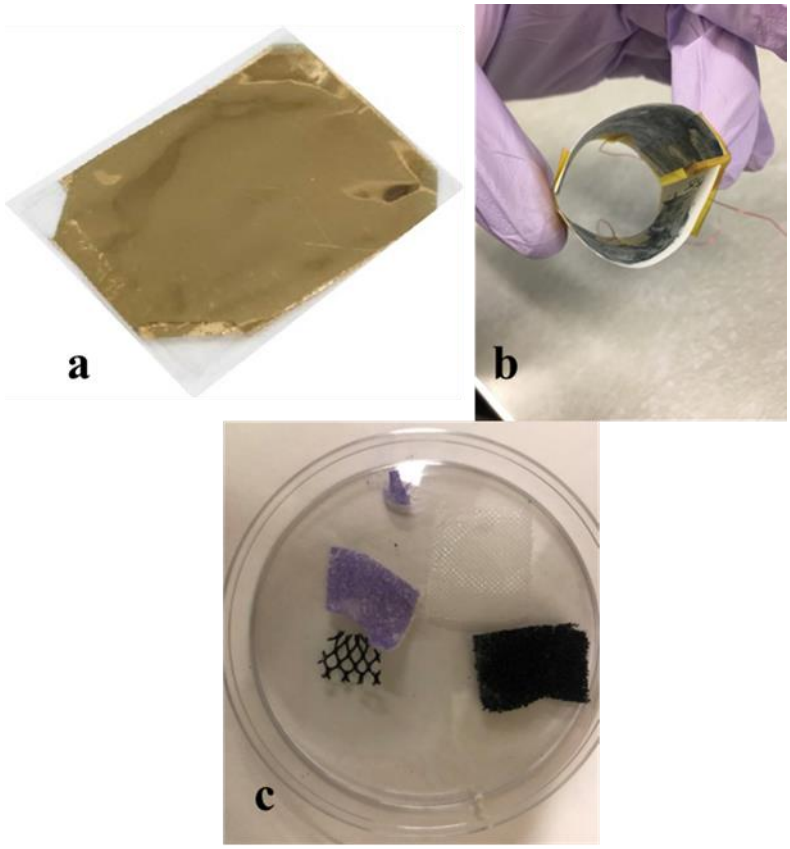


Figure 9, *(a) Au/PET/EVA/FEP device used for energy generations. (b) Paper/PLA/PEDOT:PSS prototype device for biodegradable energy harvesting applications. (c) Material breakdown of a commercially available air filter for evaluation of its electrostatic properties*

In chapter 2, the concept of using hydrogen as a fuel source is introduced and the production of hydrogen by the water splitting mechanism using the electrolysis process is discussed. Electrostatic polymers and their use to generate energy is explained and utilized to construct a hydrogen generating system based on the electrostatic polymer in **Fig. 9a**. The geometry design and system fabrication process are then conducted and the prototype device is characterized experimentally, including electrical properties such as voltage and current outputs. Experiments assessing hydrogen generating capabilities are tested and results are compared to other similar devices and applications.

Chapter 3 presents the exploration of other electrostatically charged materials for possible enhancements in energy harvesting applications. Biodegradable materials are first discussed to decrease the amounts of toxic wastes in the environment. Material choices and their synthesis processes are examined first and preliminary experiments are performed to evaluate their potential usages for energy harvesting applications as shown in **Fig. 9b**.

Another material that can store high electrostatic charges is the silicon dioxide material with the heat resistant property and possible IC compatible processing. As a demonstration for the proof-of-concept, a preliminary deposition process is tested and characterized.

In chapter 4, electrostatic polymers for the air filtration applications are studied by evaluating industrial electrostatic polymers and their efficacy in air purification systems to combat COVID-19. Various methods in air filtrations are first discussed, including the advantages of using electrostatically charged polymers. Manufacturing processes of electrostatic polymers have been examined with possible integration procedures to the air filtration system. The electrostatic properties of commercially available air filters are tested and modified to improve the electrostatic property as shown in **Fig. 9c**. Finally, a generic commercial air filter is dissected to evaluate the electrostatic property of its individual components toward a better filtration system.

Conclusions for the dissertation are discussed in Chapter 5. They include the evaluation of a polymer-stack piezoelectret device capable for converting mechanical energy into electrical energy. A paper base device is also presented for energy harvesting applications with a focus on biodegradable materials. Finally, a study of electrostatic performance for materials commercially available in air filtering products is presented.

2 Electrostatic Polymer for Energy Harvesters

2.1 Introduction

2.1.1 Hydrogen as a Fuel Source

The world currently uses fossil fuels as its primary source of energy [37]. Scientists estimate that there are about 50 years left of fossil fuel reserves, further escalating the need to find alternative energy sources [38], [39]. Besides being an exhaustible resource, the use of 1 Kg of fossil fuels produces 3.2 Kg of CO_2 [40]. This CO_2 gas is known to cause adverse effects such as the greenhouse effect, stratospheric ozone depletion, acid precipitation, and smog [39]. Additionally, the extraction of fossil fuels has led to catastrophic events such the Deepwater Horizon oil spill in 2010 which has environmental effects still not fully understood. Hydrogen is a promising fuel source for the world's energy needs based on its conversion efficiency, easy transportation, and various phases of storage. Its combustion does not produce harmful greenhouse gases that contribute to the environmental problems discussed previously [40]. The major current hydrogen source is from greenhouse gases which hinders its viability as a source of clean energy [41]. Hydrogen from water splitting only requires water and a source of voltage at 1.23 V to catalyze the reaction [42]. Furthermore, water covers 70% of the Earth's surface and is a renewable resource [43]. As such, the ability to produce hydrogen via water splitting has the potential to use abundant resources to produce clean energy [44].

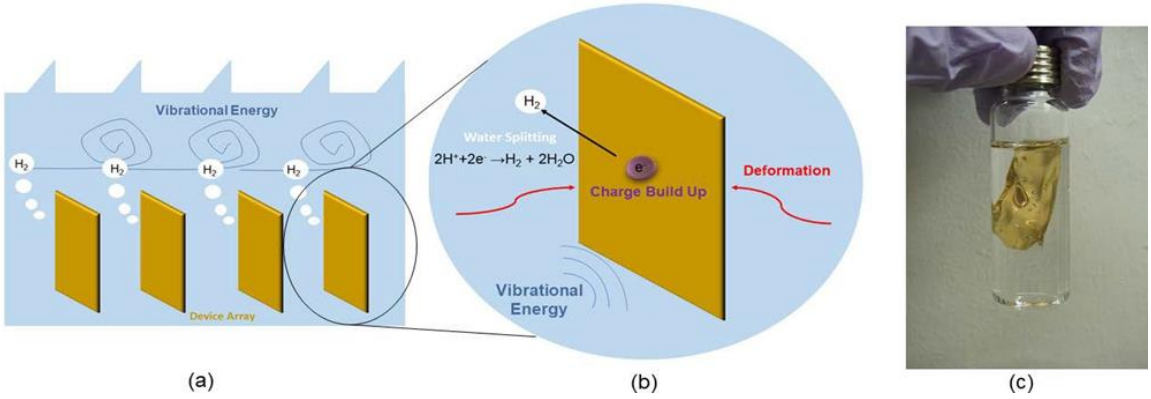


Figure 10, *Energy Harvesting Principle of this work. In the far left an array of piezoelectret devices are disturbed by vibrational energy in the ocean. Middle image shows that this vibrational disturbance causes charge generation on the surface of the devices. The charges start the electrolysis process and hydrogen is released. The far-right figure is the experimental setup image of this concept.*

2.1.2 Water Splitting and Energy Harvesting

Water splitting has gained considerable interest as a source for energy production from hydrogen based on its use of water - an abundant renewable resource, as its main reactant. Other methods for water splitting include chemical and thermochemical water splitting, electrolysis, and photocatalysis [45][46][47]. In most cases, the large-scale application of water splitting is hindered by multiple engineering and scientific barriers. For example, the chemical water splitting process suffers from producing harmful CO_2 by-products [48]. The thermochemical splitting process requires temperature upwards of

2000K, while the electrolysis scheme has high energy and investment costs. The photocatalysis process generally only uses 4% of the solar spectrum which greatly limits its use as well [49].

Electrostatic polymer systems also known as piezoelectric devices can convert mechanical stimuli into voltage through the movement of dipoles in the material [50]. They can also perform the reverse process to convert voltage into mechanical movements. This piezoelectric effect has been used to create widespread modern technologies such as microphones, speakers, and resonators [51]. Piezoelectret devices are newer class of devices that are primarily made of charged polymers which display similar mechanical to electrical conversion characteristics as those of piezoelectric devices. They are constructed by charging polymers with many air gaps which can be polarized by a high voltage source such as the corona charging process [52]. Their recent development has been fueled by their ease and versatility specifically for flexible electronics and energy harvesters [23].

Piezoelectric ceramics have been used to demonstrate water splitting using ultrasonic waves and turbines in water as the input energy [53]. Mechanocatlysts materials such as ZnO microfibers, $BaTaO_3$ micro-dendrites, and various metal oxide powders have been applied [19], [21], [54]. These devices suffer from issues such as long processing time and high processing temperature requirements, and they are generally expensive to produce hydrogen [55]. Here, we use a simple method to fabricate piezoelectret devices which can be excited by vibrational disturbances in water to generate hydrogen. Our choice for the controlled vibrational motion is the ultrasonication. The proposed scheme is illustrated by **Figure 10.**

It has been calculated that if only less than 0.1% of the renewal energy in oceans could be converted to electricity, it will satisfy and surpass the present world demand for energy of more than five times over [41]. Given this, it is attractive to consider engineering systems that can harvest energy produced by tidal motions every day. As technology advances, this energy resource can become a significant source of renewable energy in the future [43], [56], [57].

2.2 Device Fabrication

2.2.1 Fabrication

Figure 11 illustrated the fabrication process. The process starts by enclosing a layer of FEP material within two 58 µm-thick PET layers using a hot-pressing method described in the prior work [7]. The 23 µm-thick FEP layer acts as a spacer where the air trapped in the structure can be charged [58]. The charging of the device is performed using the corona charging method. The PET/EVA/FEP sandwich has one side grounded and the other side near a corona needle which applies 15 kV. This high voltage causes the breakdown of the air in the structure which creates electrical dipoles [59]. After the charging process, the device requires the metallization layers to generate voltage [60]. Au was chosen for its chemical inertness as opposed to other metals which could react with water. A 50 nm-thick layer of gold was deposited using a customized DC magnetron sputter deposition system.

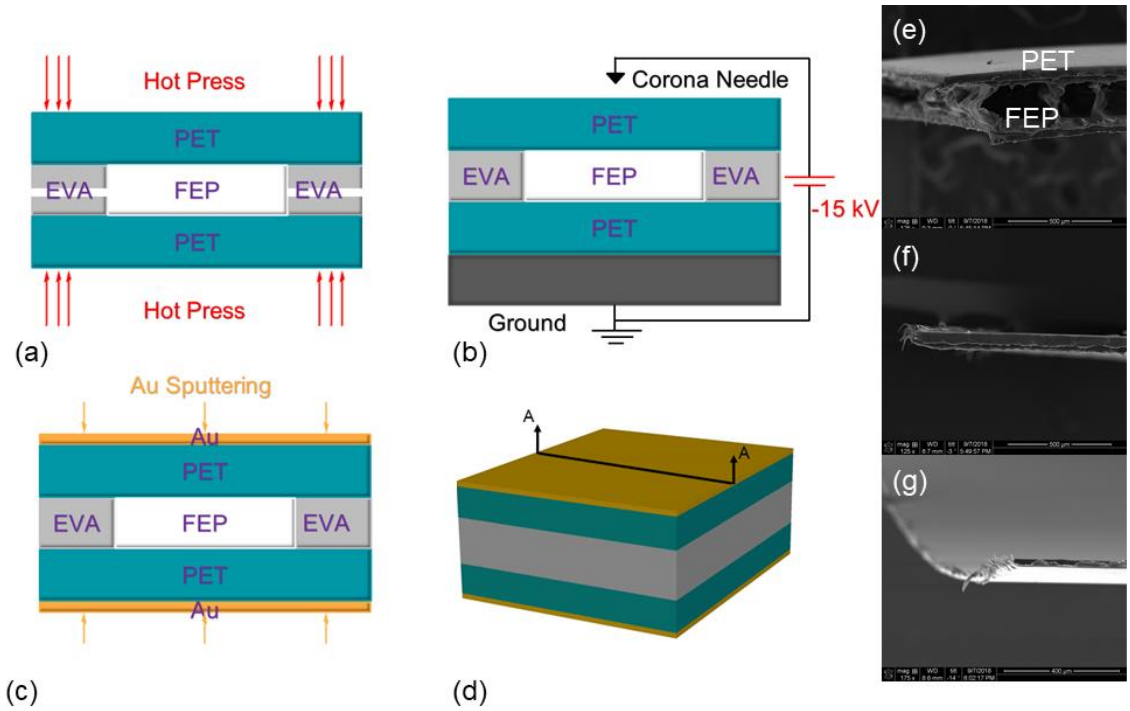


Figure 11, *Device Fabrication and Geometry. (a) The device is made by creating a stack of materials. The stack is compressed on a hot plate. The heat seals the EVA layers together. (b) The device is charged using the corona charging process. A 15kV voltage is applied to the device which ionized voids within the charge storage layers. (c) The device is covered with Au using a sputtering process for the Au electrode to collect charges. (d) 3D computer rendering. (e) SEM image of the device for the cross section (A-A). (f) PET SEM image, (g) FEP SEM image*

2.2.2 Device Geometry and Working Principle

The charges that are stored in the device are accessible by deforming it. **Figure 12** shows the four-step process. First the system is at rest and charges are fully balanced [61]. A force that compresses the device causes the charges within the polymer to come closer together. As the polymer charges come closer together, charges in the metallic layer are pushed out of the system. These are charges that can be collected to induce a current. When the compression ends the device returns to equilibrium, charges in the polymer are far from each other, and charges in the metallic layer are not disturbed.

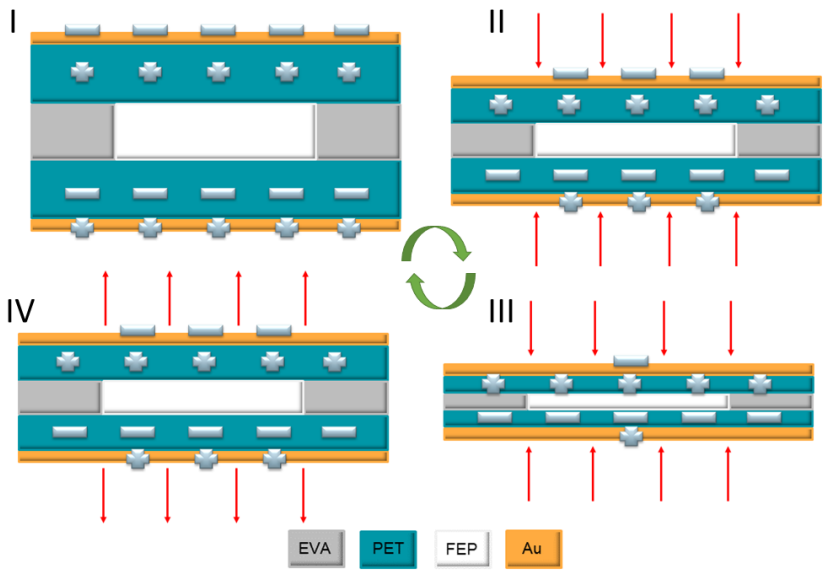


***Figure 12**, Device Working Principle. I: device at rest. II: device is compressed, and polymer dipole forces cause charges in the metal layer to release. III: maximum compression occurs, and no more charge can be released. IV: Device is released from compression and charges re-accumulate on the metal layer.*

2.3 Results and Discussion

2.3.1 Voltage and Current Characteristics

The device function was first tested using a manual pressing process. The device was connected to a voltage measurement system using wires and the voltage response was recorded over time. **Figure 13** and **Figure 14** show the results. The reverse and forward connection are tested to verify the validity of the signal acquired from the measurement system. They prove the signals are from the device rather than artifacts of the measurement system. The manual pressing process also serves to confirm that the device can generate voltage higher than the 1.23 V to split water [62], [63]. The variations in the voltage and current outputs mainly come from the random manual pressing process. In general, the voltage outputs are not centered at zero volt due to the floating voltages on the device. The back and force voltage and current outputs are common features for vibration-based energy harvesters due to the compression and releasing processes, respectively. **Figure 15** shows an optical image of the device.

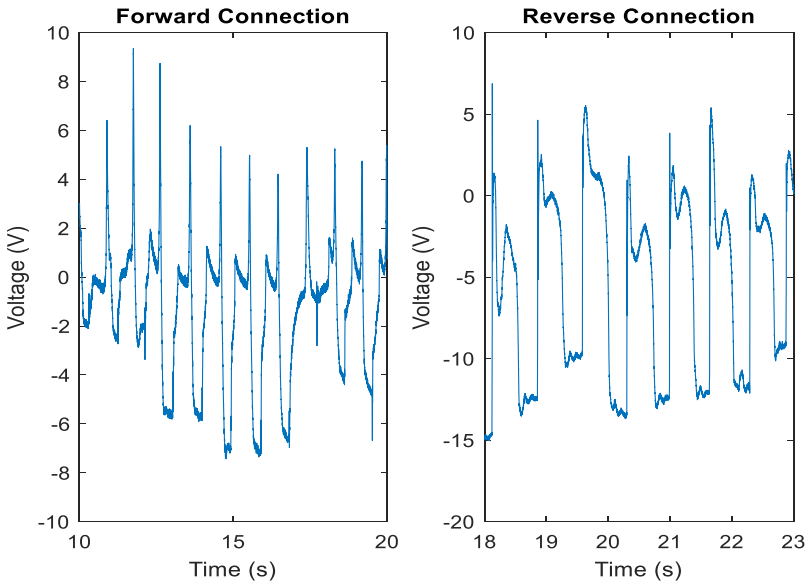


***Figure 13**, Voltage Characteristics via Manual Pressing. Peaks correspond to a manual compression of the device using a finger. Forward and reverse connection are tested to confirm the system is operating due to the mechanical deformations instead of artifacts.*

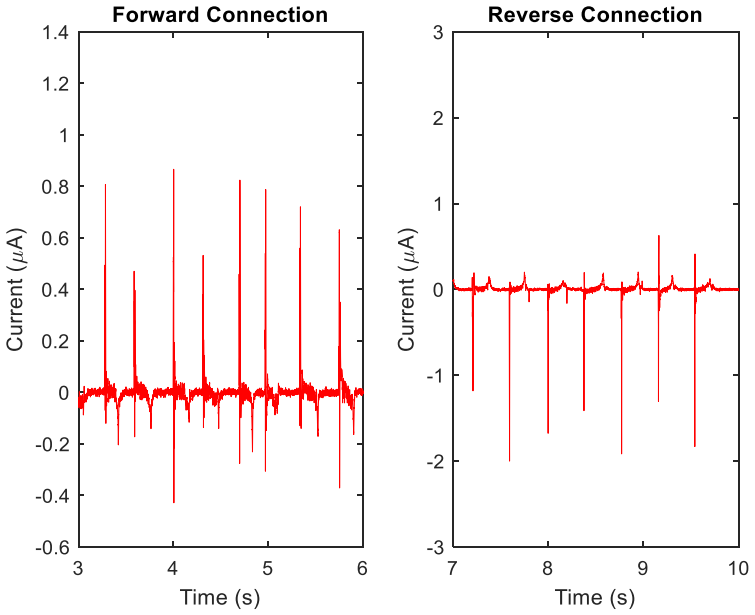


***Figure 14,** Current Characteristics via Manual Pressing. Peaks correspond to manual compression of the device using a finger. The forward and reverse connection are tested to confirm the system is functional instead of artifacts.*



Figure 15, *Optical Image of a Fabricated Device. The gold layer is opaque and prevents the other polymer layers from being seen. The corners show the PET/EVA in the device.*

2.3.2 Ultrasonication Voltage

In the interest of using the device to harvest vibrational energy in liquid medium, the voltage response was tested under ultrasonication in DI water. The device was placed in a standard gas tight Gas Chromatography vial partially filled with DI water. Afterwards, an N_2 gas purge was performed [64]. The entire vial was then submerged in an ultrasonic tank and exposed to ultrasonication at 40 kHz for various time periods. Bubbles made of gases can be visually seen on the surface of the device electrodes. **Figure 16** shows the resulting voltage response with output voltage in the 4-7 V range due to the floating potential. The inset of the figure shows the responses from a 2-millisecond time period.

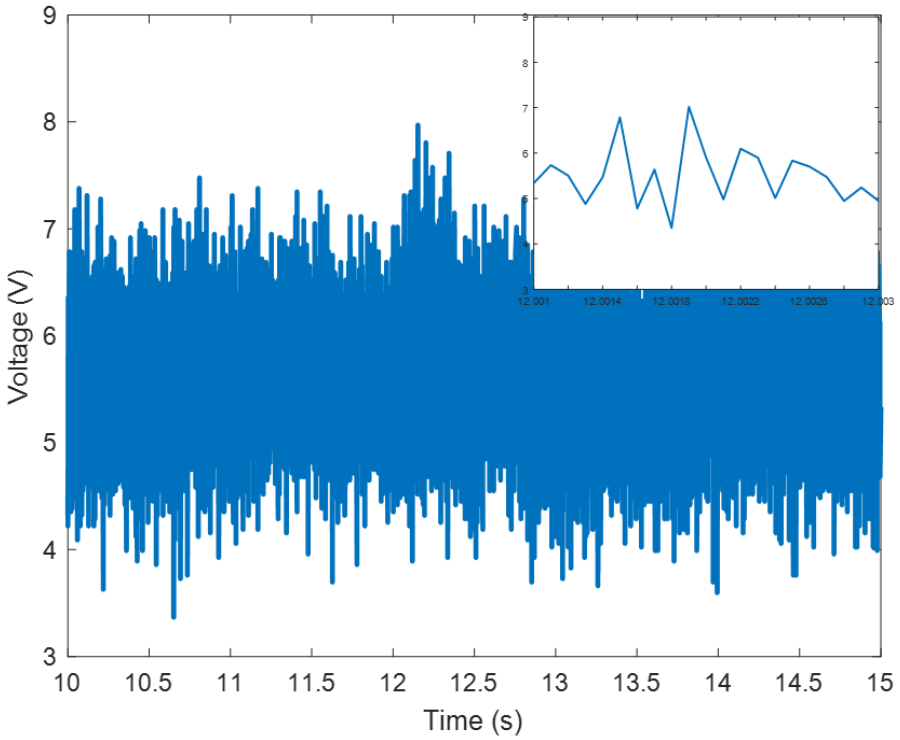


Figure 16, *Ultrasonic Voltage Characteristics. The inset shows a narrower time range during the operation.*

2.3.3 Surface Charge Potential

The surface charge potential of piezoelectret devices is used to study their stability over time. For example, some prototype devices show good stability after 50 days with quasi-permanent electrical charge [65]. The surface potential was plotted in **Figure 17**. A longer study period would be required to view the flatline surface potential of the device. However, it is assumed that the value at stability would be quasi-permanent and allow for the continued device operation [66]. Over time charges stored in the device can be neutralized by contacts with particles such as dust or moisture. Applying corona charging for a longer time and periodically will increase the lifespan of the device.

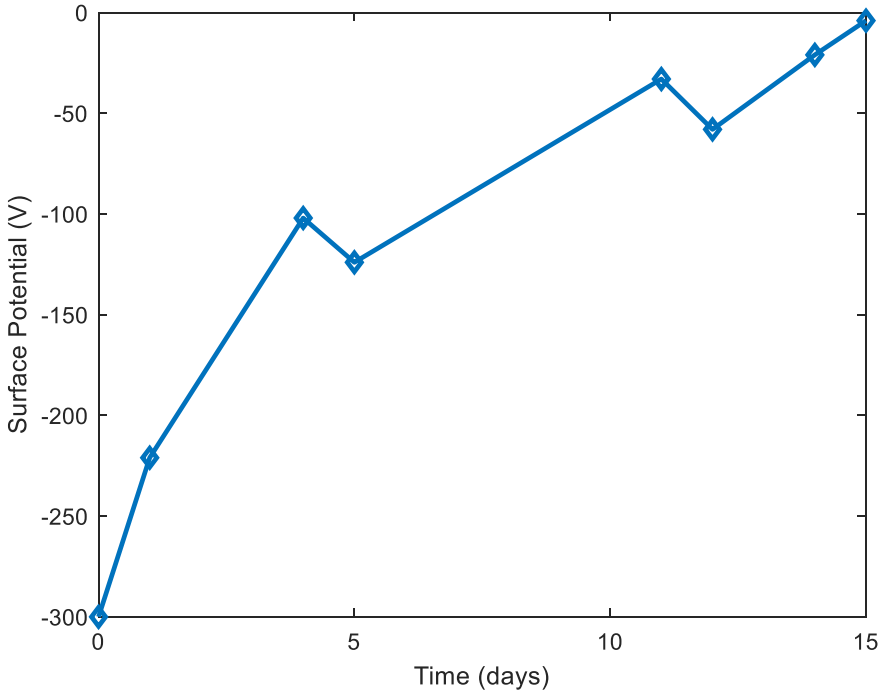


Figure 17, *Surface Potential Decay. The surface potential starts at 300V after the initial corona charging process. There is a total decay after 15 days.*

2.3.4 Gas Generation Quantification

Gas Chromatography (GC) measurements were used to verify the H_2 generation capabilities of the prototype device as a standard test [67]. First the PET/EVA device is submerged in deionized water. The chamber is then flooded with nitrogen to remove outside contaminates. In the future, a theoretical value for the voltage generated can be calculated by modeling the ultrasonication force as a bending force on a cantilever-type beam structure to have the full understanding of the energy generation process. The generation of hydrogen over time could be calculated by the resulting voltage, current and the device area. After the sonication process, the gas in the headspace of the GC vial was extracted using a gas tight syringe and injected into a GC equipped with a conductivity detector and an Argon carrier gas.

Table 2 *Hydrogen Generation Results*

Sample	H_2 Generation (ppm/hr.)
PET/EVA	0.00
Au Nugget	0.00
Water	0.00
Device	12.99

Table 3 *Generation Comparisons in Literature*

Catalyst	H_2 Generation (ppm/min)
This work	0.217
ZnO [11]	0.375
$BaTiO_3$ [11]	0.520
NiO [10]	0.001

The device is composed of PET/EVA and gold. As a control and validation test, these components were tested under the same conditions to validate that the H_2 production was a result of the device subjected to sonication with results shown by **Table 2**. Previously, other works using piezoelectric ceramics such as ZnO and $BaTiO_3$ have also been demonstrated for hydrogen generations as shown in **Table 3** for hydrogen gas generation rates of 22.5 and 30 ppm/hr [68], [69]. The table only provides a very rough comparison as the sonication frequency used in these reports is the same but the power, distance, and the shape and size of the devices will all affect the generation rates. Roughly speaking, this indicates that our prototype device produces hydrogen on the same order of magnitude as those of other systems without using complicated fabrication methods. For example, some of those hydrothermal methods require over 72 hours to make piezoelectric ceramics [70], [71]. Additionally, the prototype devices can split water directly on the surface of electrodes without the need for a transformer or rectifier needed in other systems [67].

2.4 Conclusions

In summary, we have demonstrated the feasibility of using a piezoelectret device as a mechanocatlysts for the generation of H_2 via ultrasonication. The device performance was characterized using voltage output measurements which supported its capacity to generate the required voltage to split water at 1.23 V. These voltages were generated using both manual and ultrasonic vibrations. The validity of the device for producing H_2 was also tested using Gas Chromatography measurements which revealed that Hydrogen gas was generated by our device under ultrasonication. Our method presents a novel way of using mechanical vibrations to generate hydrogen as the energy source in the form of using fluidic mechanical motion to generate electricity for the electrolysis process. Furthermore,

there are two main contributions to engineering applications. The addition of FEP inside the PET void is the first of its kind. The results of the work suggest that other piezoelectret devices could benefit from the addition of this polymer layer for increased surface areas to store induced charges for higher energy generations. For verify this, a study where the device is fabricated without the FEP would be conducted in the future. Secondly, this work reports the first use of a polymer piezoelectret to catalyze a chemical reaction and to generate hydrogen using electrolysis. The results of this work mean that other piezoelectret schemes should be investigated for their catalytic properties. Water splitting is just one of the many potential chemical reactions that could be induced by piezoelectrets. Other potential usages may include the usage of piezoelectret devices to passively catalyze a variety of chemical processes and remove the need for external voltage sources. Lastly, the small-size device study does not yield a practical application. Ultrasonication was chosen in lieu of an unavailable wave generation tank that could yield large outputs for more practical applications. The energy conversions from the ultrasonic generation to the mechanical deformation, and to the chemical generation will results in losses in energy and should be carefully designed and characterized for the future work.

3 Biodegradable and Ceramic Piezoelectrets

3.1 Introduction

This chapter discusses biodegradable and ceramic piezoelectret devices as possible system improvements. Biodegradable materials are of interest due to the rising costs of climate change associated with toxic plastic wastes in the environment. Ceramic piezoelectret devices are of interest due to their superior stability at high temperature and feasibility to store more induced charges. Using ceramic materials enables manufacturing at high temperatures with a wider range of operating conditions.

3.2 Biodegradable Device

The materials used in this section have been selected based on their electrical and mechanical properties. Given the issues that plastic waste has caused in the environment, there is a reason to use materials that have a lesser impact on the environment [72]. This work uses biodegradable materials to create an electrostatic polymer system for energy harvesting. **Figure 18** shows the geometry of the system.

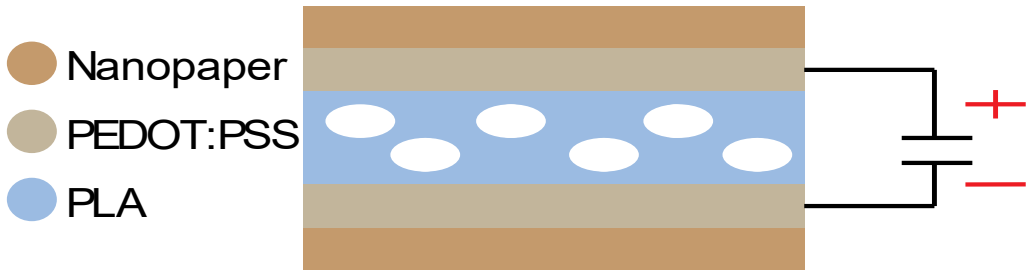


Figure 18, *Biodegradable Polymer System. The PLA layer is biodegradable and filled with voids which can be ionized. The nano-paper is made of cellulose and provides mechanical supports to the device. PEDOT: PSS is a conductive polymer which collects the charges generated by PLA.*

The PLA is a corn-based polymer that is known for being compostable [73] as most compostable eating utensils are made of PLA. The material easily forms voids which can be ionized [74]. PEDOT: PSS is a conductive polymer, while the biodegradable properties of PEDOT: PSS are mostly debated [75]. For the purposes of this work, it was assumed that the material would degrade in the environment. In addition, it was chosen because it can be synthesized at low temperatures and adheres well to PLA [76]. Finally, it was chosen because its conducive properties allow the charges from the PLA to be collected for energy harvesting. Nano-paper is an alternative name for paper made of cellulose [77]. Cellulose are the fibers that compose plant material. This layer is used as the structural layer. Without it, the nano-paper and cellulose would be too thin to withstand the mechanical deformation [78]. An added benefit to using nano-paper is that it can be made transparent [79] as transparent devices may be less cumbersome and applicable when the appearance of the device is important [80]. The combination of the three materials creates a device that has good electrostatic properties, mechanical stability, and can generate electrical energy by converting mechanical deformations to electrical outputs [81][82].

3.3 Manufacturing

The following image shows representative steps of the manufacturing process. The materials are purchased in raw forms such as powder and pellets. The transition from the raw form to thin films depends on the physical state and chemical properties of the material. Various chemicals and physical processing equipment are used to initiate the transition. **Figure 19** demonstrates the processes.

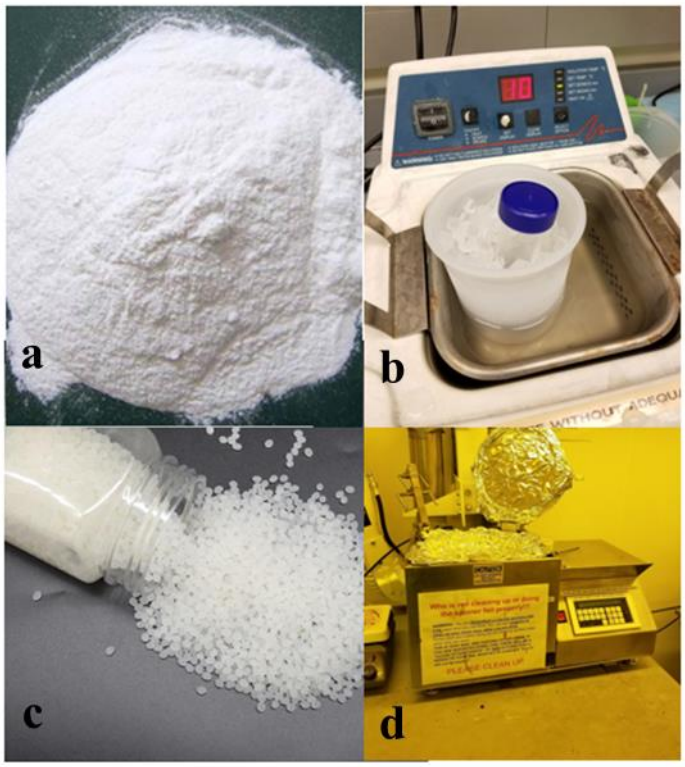


Figure 19, *Cellulose and PLA Process: (a) cellulose powder prior to processing; (b) cellulose in an ultrasonic ice bath which separates the microfibers; (c) a bottle of PLA pellets prior to processing. (d) the photoresist spinner used to create PLA thin films.*

The process was created based on a review of various papers. The cellulose substrate process begins with cellulose powder [83]. The powder goes through various processes such as chilling and a centrifuge cycle to create a film [84]. The PLA film process begins with PLA pellets. The PLA pellets are dissolved in chloroform and the resulting liquid is spun into a thin film by using a photoresist spinner [85], [86]. The PLA is spun onto the cellulose substrate. The cellulose layer is difficult to create as shown in the optical photos in **Figure 20**. In this case, process (a) is a cellulose film without sonication and the clumps of cellulose are visible as shown in **Figures 20 (a)**. Process (b) is a cellulose deposited after the sonication process in an ice bath as shown in **Figures 20 (b)** by using 0.22g of cellulose powder bathed in .8571 g of Urea, .5 g of NaOH, and 5.786 g of deionized water. After two hours of sonication the solution is cast using a pipette onto the petri dish and coated in ethanol. It is found that process (b)is preferable due to its uniform

properties as opposed to the clumping seen in case (a). **Figures 20 (c) and (d)** are the SEM images showing the difference between the fiber morphologies of the layers. The fibers in (a) are thin and around 10 µm in length with a small diameter. The fibers in (b) are flattened into a sheet.

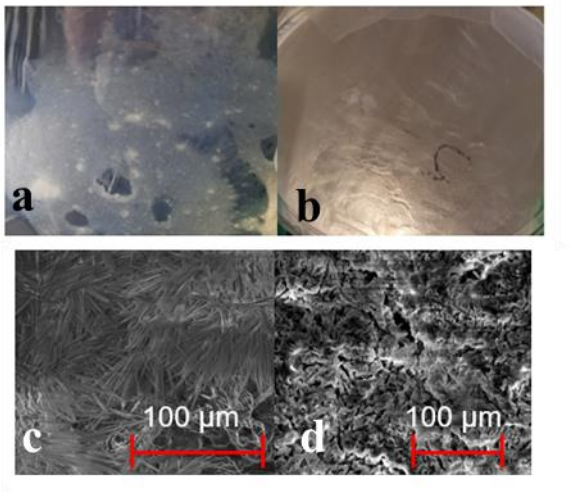
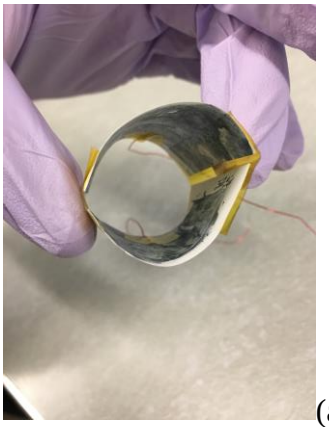
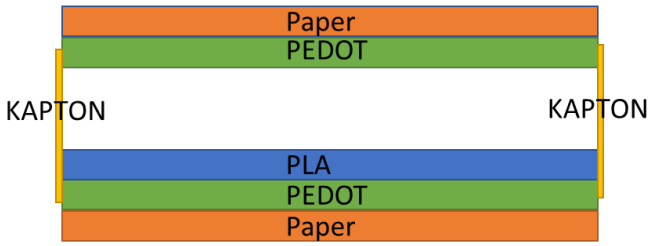


Figure 20, *Cellulose Optical and SEM Images: (a)(b) optical photos of the cellulose films for process (a) and (b), respectively. Process (b) is preferable due to its uniform properties as opposed to the clumping seen in (a). (c)(d) The SEM images showing the difference between the fiber morphologies of the layers.*

Cellulose can be deposited transparently but the microstructure photos show that the fibers are stacked upon each other instead of elongating and tangling for structural stability. As a result, the substrate created was brittle and broke immediately when touched. HP Multipurpose 8.5”x11” 92 brightness office paper was then used to continue the investigation. **Figure 21a** shows the schematic diagram of the new structure and **Figure 21b** shows the prototype of the device.



(a)



(b)

Figure 21, *Biodegradable Device Prototype. (a) The prototype is held together using an insulating Kapton tape. The PEDOT:PSS is seen in the black ink. (b) Conceptual drawing of the device.*

The office paper is utilized to replace the proposed cellulose paper for better mechanical stability. The PEDOT: PSS is the dark layer in the figure. This prototype was corona charged for 10 minutes at a 5 cm distance using 21 kV so the voids in the PLA could be ionized [87], [88]. Afterwards, the office paper was cut into pieces and drop-coated with PEDOT:PSS.. A layer of PLA was then spin-coated onto the surface. The paper/PEDOT/PLA substrate was then corona charged to impart charges in the PLA layer. Two paper substrates are needed (Figure 21b). The second paper substrate is drop-coated with PEDOT:PSS. Afterwards a wire is attached to both substrates on the PEDOT:PSS surface area. Kapton tape is attached to the edges (21a) of the substrates to keep the pieces together.

3.4 Prototype Device Fabrication and Testing Results

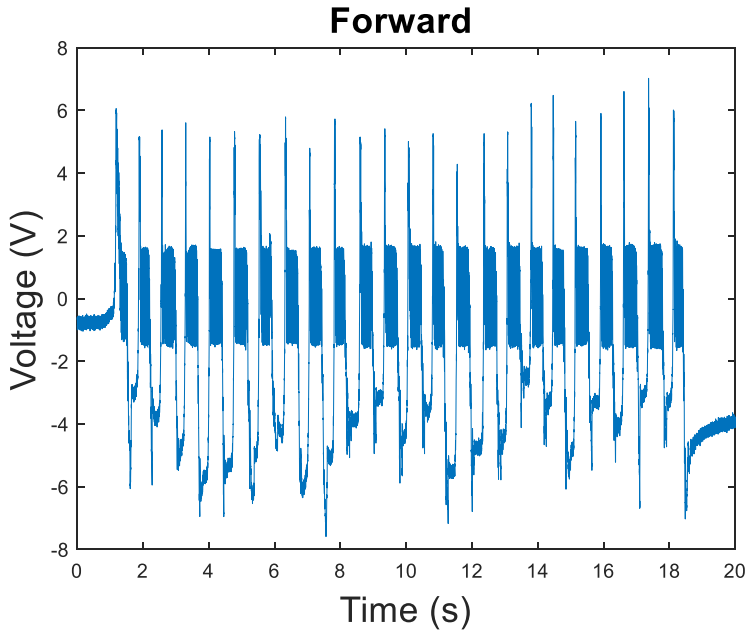


***Figure 22**, Biodegradable Prototype Response. The peaks correspond to manual compression of the device using a finger. Peak to peak voltage is about 12V which is well over the voltage required to power most small electronics.*

The voltage response of the prototype is demonstrated by **Figure 22**. The voltage response corresponds with continuous manual deformation of the device powered by a finger. From the graph, we see output peak-to-peak voltage of 12V which is high enough to power most popular electronics [89].

	Surface Potential (V)	
Sample	Initial Charge	Day 2
Cellulose/PLA	148	11
PI Tape/ Cellulose/PLA	39	11
Cellulose/Spin Coated PLA	94	2

Figure 23, *Biodegradable Substrate Charging. Results show quick surface potential decay which is unfavorable for long term stability of the system. The samples differ in substrates because cellulose must be deposited on a structural layer. Certain substrates allow storing more charges than others.*

Figure 23 shows results of charging various films used in the biodegradable device. The cellulose/PLA combination shows the highest amount for a corona charging process of 5 cm, 10kV, and 1 minute. The drop coating process involves dissolving the PLA in chloroform at room temperature by mixing the two in a magnetic stirrer at its medium setting for 4 hours. After the PLA is fully dissolved, the solution is poured onto a petri dish. The spin coating process takes the dissolved PLA into a 10 mL dropper and 5 drops of solution are deposited onto an Si wafer. The wafer is then spun at 1000 rpm for 25 seconds. The results show that a drop coated deposit of PLA holds more charge than the spin coated layer. Visually, the results are consistent because the drop coated layer is much thicker than the spin coated layer and thus could potentially hold more charge. An SEM image can be taken to measure the thickness of the spin coated layer in micrometers. The PI tape sample shows that charging the device with the structural PI tape yields a lower surface potential. This is consistent with the insulating properties of the PI tape [90].

3.5 Biodegradable Device Future Work

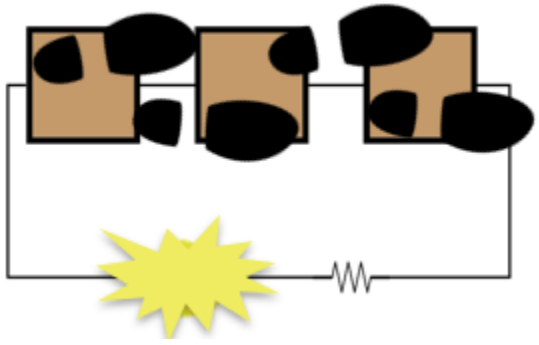


Figure 24, *Footstep Powered Lighting. Footsteps along an array of devices cause compression which releases charges from the devices. These charges can be used to light up nearby bulbs.*

This work shows the first use of a biodegradable piezoelectret device for energy harvesting using mechanical inputs. Future engineers can consider more environmentally friendly and biodegradable materials for their applications based on the success of devices that show the results in this work. **Figure 24** shows a theoretical framework for footstep powered lighting. An array of these biodegradable devices could be laid out so that the disturbance from someone walking on them can power a nearby light source. The number of devices needed is dependent on the power requirements of the light source. For example, if the light source requires 6V to operate and the device can provide 3V, 2 devices connected in series would be used for the light source. The current was not measured explicitly in the preliminary study but previous studies had shown that piezoelectret schemes suffer from low current output. The way to increase the current is to increase the charging time of the device and to increase the overall device surface areas. To meet a certain current requirement, multiple devices can be connected in parallel.

3.6 Ceramic Piezoelectret

So far only carbon-based polymers were discussed. During the span of this work, there was an interest in the fabrication of a fully ceramic piezoelectret. A benefit of using ceramic materials is that they are stable in temperatures that far exceed most polymers and some ceramic materials can store more charges than those of polymeric materials [91]. SiO_2 is the ceramic of choice because it has one of the highest surface charge densities of any electret materials as shown in **Table 4**. SiO_2 shows orders of magnitude larger charge density than those of the state-of-the-art polymeric materials such as PTFE. CYOTP is cyclic transparent optical polymer.

Table 4 *Common Electret Materials and their Charge Density.*

Electret	Charge Density
SiO_2 [92]	15 mC/m^2
SiO_2 [93]	5 mC/m^2
Parylene HT [94]	3.7 mC/m^2
CYTOP [95]	1.4 mC/m^2
FEP [9]	1 mC/m^2
PTFE [96]	0.5 mC/m^2

SiO_2 is commonly grown using thermal oxidation or chemical vapor deposition. Thermal oxidation yields the most uniform results however it takes many hours to deposit a thick film. Chemical vapor deposition (CVD) and plasma enhanced chemical vapor deposition (PECVD) are much faster but they yield lower quality films. **Figure 25** shows the proposed structure.

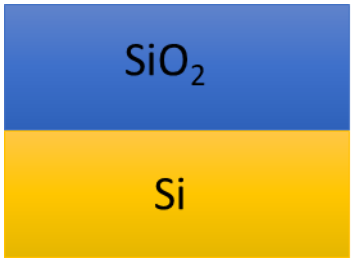


***Figure 25**, Illustration of Ceramic Piezoelectret. SiO_2 Air can be ionized and charges can be stored on the SiO_2 layer.*

This preliminary work is to verify the electret property of SiO_2. SiO_2 is grown by thermal oxidation of a Si wafer. An added benefit of using the SiO_2 as an electret is its high temperature stability. When adding a metallic layer for charge collection on an electret, choices are generally limited using polymers since they melt at temperatures much lower than the deposition temperatures for metals. SiO_2 has been used for many decades in IC technologies, so there are many more options for processing [97], [98].

3.7 Fabrication and Characterization

Figure 27 shows an SEM image of one of the SiO_2 depositions on a removed portion of an Si wafer. The process was 1200ºC and 2 hours. Cracks may be attributed to the wafer cleaving process. Final thickness of the film was not measured by assumed to be close to 1 µm based on standard wet oxide growth rates. The cracks show there were stresses in the film [99]. The defects may be helpful because they can become charge storage sites [93].

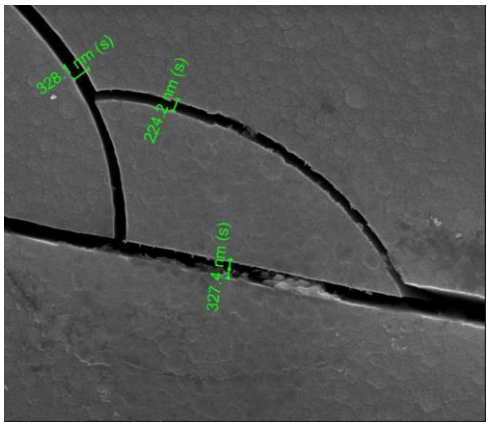


***Figure 26**, SEM Image of SiO_2 Layer. Cracks suggest errors in the growth process but can also be used to store charge.*

Previous work suggests that the cracks may be detrimental to adding metallic charge collecting layers [100]. Depositing a metal is best on a planar surface so that the metal makes uniform contact. The fabrication process requires control so that the films produced can provide the desired properties such as charge storage capability. **Figure 28** shows Powder X-Ray Diffraction spectrum for a deposited SiO_2 film.

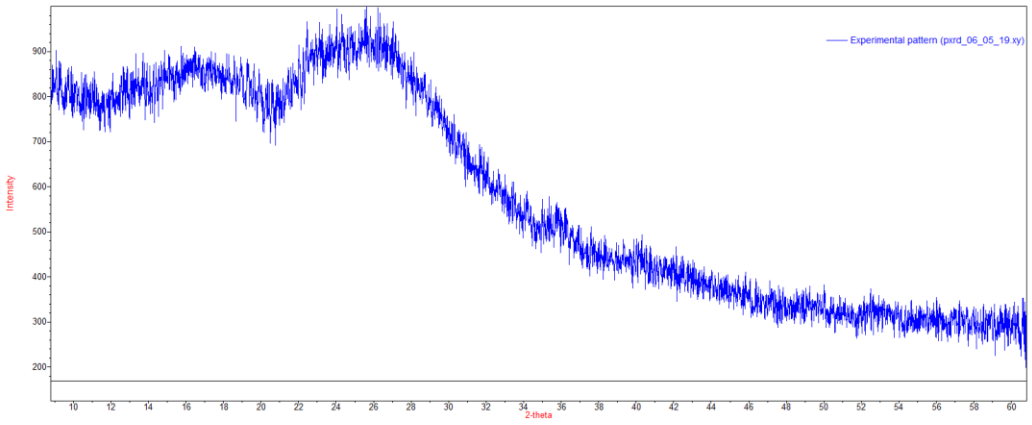


Figure 27, *PXRD Results for the SiO_2 Film. The peaks correspond to crystallinity in film layers.*

Literature shows that as the crystallinity of the film increases, so does the charge storage capabilities [101]. Crystallinity is measured using PXRD. The PXRD spectrum gives shows peaks at various locations based on the material. If this graph had a higher peak at 24 2-theta, it would mean that the crystallinity was higher. This would theoretically correspond to the charge storage capability of the SiO_2 layer. Ultimately the PXRD characterization is measurement step that is taken to predict the performance of the SiO_2 as an electret.

3.8 Ceramic Device Conclusions and Future Work

Previous studies on the electret properties of SiO_2 and its high temperature stability make it a material worth studying for energy harvesting purposes. Future work would require establishing a reliable fabrication process that would yield SiO_2 at the desired thickness and quality for the high charge density found in other works. The SiO_2 would be deposited then it would be charged using the corona charging process as previously mentioned in this work. Charge longevity would also be studied. Once a process is established, the next task would be to choose a metal charge collecting layer and a scheme for harvesting energy. For example, an aluminum metal layer could be deposited. Afterwards the energy harvesting capabilities for the device could be determined by applying a force using a motor so that the force is consistently applied.

4 Electrostatic Polymers for Air Filtration

4.1 Introduction

4.1.1 Air Filtration and Electrostatic Polymers

The Covid-19 pandemic caused mass interest in air filtration systems [102]. **Figure 29** shows established methods of particle filtration [103]. Inertial and diffusion effects capture large particles efficiently [104]. The microscopic size of Covid-19 particles makes it a perfect candidate for electrostatic filtration [105] as electrostatic filtration dominates the capture of small particles [106].

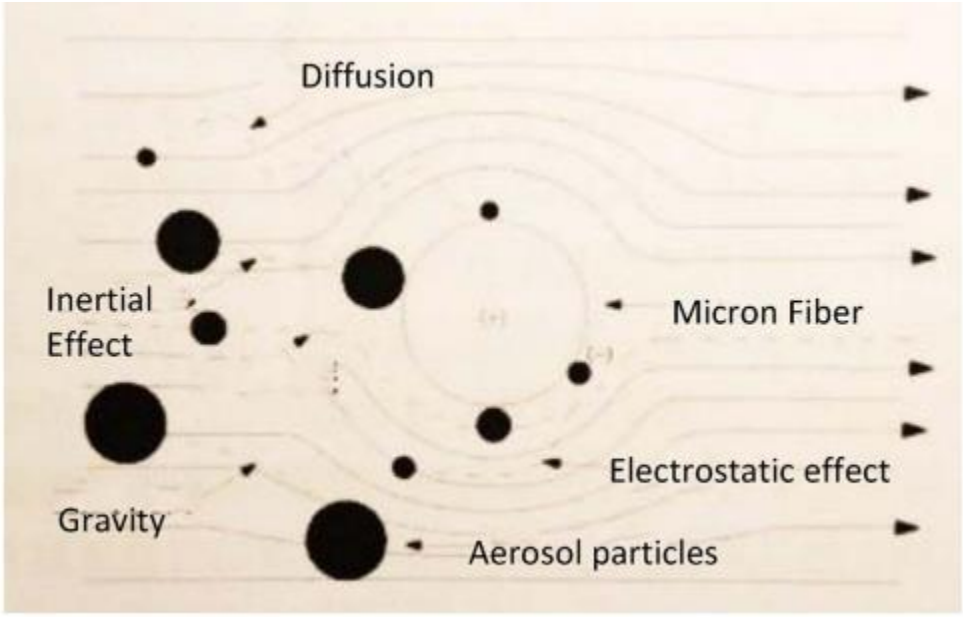


***Figure 28**, Air Filtration Schemes. The micron fiber is positively charged in the middle. High to low concentration distribution of particles causes filtration by diffusion. Gravity causes inertial effects which can filter large particles. Electrostatic effects cause attraction to the micron fiber and thus electrostatic filtration.* [104]

Electrostatic polymers in filtration applications are primarily fiber based. Many may employ a variation of electrospinning process [107]. The electrospinning process achieves two major milestones for air filtering applications. Firstly, it created micro-thin fibers that act as a web to physically filter out large particles [108]. This enables the inertial and diffusive filtering that was well-demonstrated. Secondly it impregnates the micro-thin fibers with charges that can be used to electrostatically filter small particles [109]. The charge of the fibers enables the electrostatic attraction of charged particles, thus increasing the filtering efficiency [102]. Major companies such as 3M and Honeywell advertise electrostatic effects in their filtration technologies [110]. Research showed the origin of the electrostatic effects are from electrostatic polymers [13]. **Figure 30** shows examples of the electrostatic advertisement regarding these manufactures. Each brand offers its own rating system for filtration. The exact filtration methods of their materials are not mentioned.



***Figure 29**, Commercial Filter Options. 3M produces four options for consumers with varying performance ratings. Honeywell provides five options with similar ratings.* [111]

4.2 Evaluation of Electrostatic Characteristics in Commercial Air Filters

4.2.1 Commercial Air Filters and Surface Charge Potential

Honeywell and 3M commercial air filters were chosen for the study because of their popularity. Nine materials were studied. They were evaluated for electrostatic activity for twenty-five days without adding any additional charges. They were also tested under two different corona charging procedures: 20kV for one minute and 20kV for one hour at 5cm distance. [112].

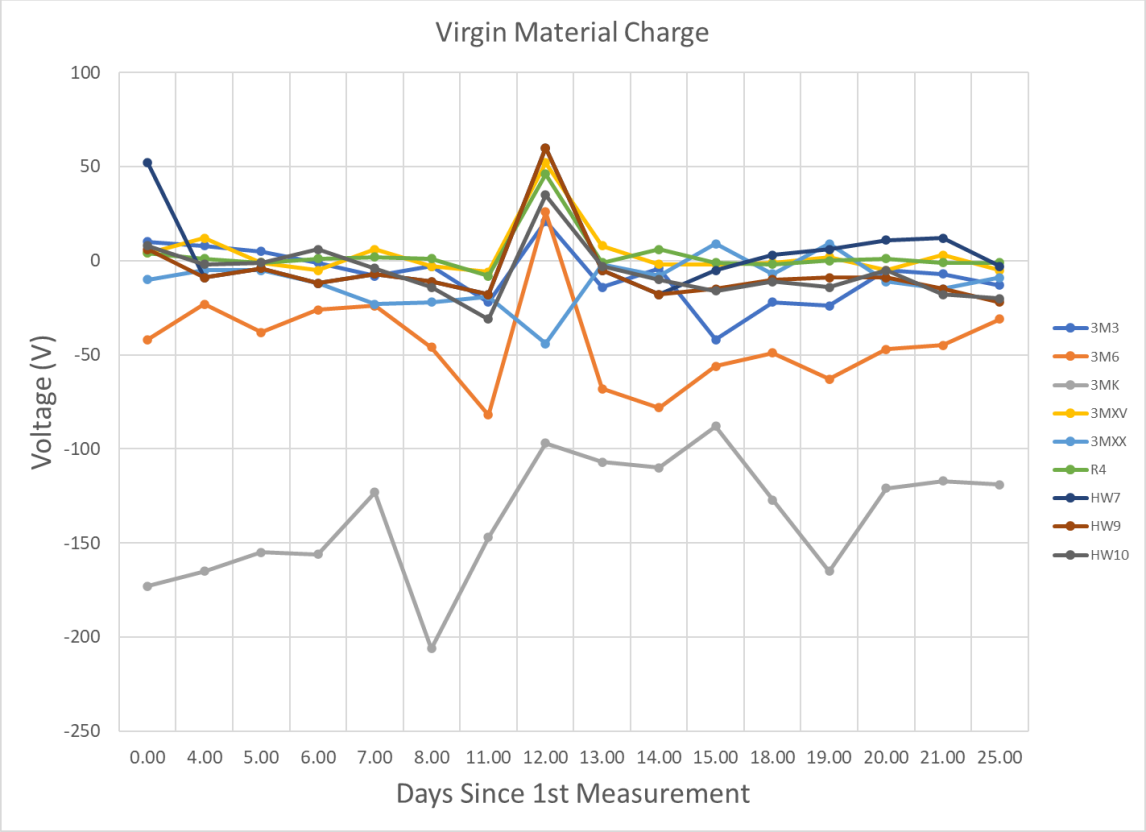


Figure 30, *Virgin Material Charge Study. Most material show negligible charge except the 3MK and 3M6. The study lasted a total of twenty-five days.*

Figure 31 shows the results of the virgin study. The electrostatic potential of the materials was studied using a Trek Model 347 electrostatic voltmeter. The voltmeter works by placing a sample under its probe. The center of the sample is labeled for a consistent measurement position. When the probe senses electric charge it will reflect that as an electrostatic voltage reading on its readout. This measurement was repeated once daily for the number of days reported in each graph, twenty-five days for example. Results show that the 3M branded 1000MPR filter possessed the highest amount of electrostatic voltage across the entire study. This suggests that electrostatic filtration is the best in this material. Conversely, some materials failed to show significant charge over the time span such as 1500MPR. All the Honeywell brand filters showed negligible electrostatic voltage. This suggests weak electrostatic filtration capabilities, although they are highly advertised. Since all materials showed some variations over the time of electrostatic potential. To improve the study, multiple locations can be measured on the sample at various times of the day to account for variability in humidity and temperature. Compiling these data would result in a more robust graph with error bars that can add reliability to the figure. This led to the evaluation of their electrostatic performance with additional charge added through the corona charging process.

4.2.2 One-Minute and One-Hour Corona Charging Study

All materials were subjected to a corona charging process of 20kV for a one-minute duration at a 5 cm distance. Since a corona charging needle was used, there is a decreasing distribution of charges as they are measured from the point of application radially. **Figure 32** shows the results of testing their surface potentials over a twenty-one-day period by storing the filter specimen in a polystyrene sample case inside of an open-air environment with a room temperature of around 70 ºF and 28% humidity.

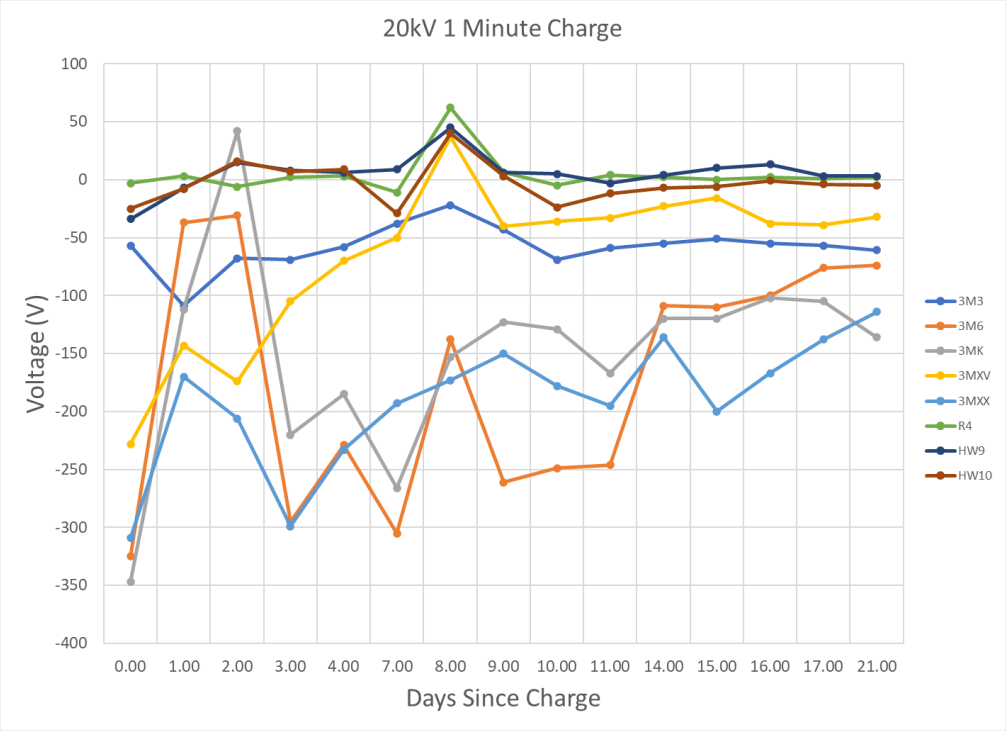


***Figure 31**, 20kV, 1-Minute, 5 cm in distance Corona Charging Study. Five materials showed significant charging capabilities: 3MXX, 3MXV, 3MK, 3M6, and 3M3. One material, R4, showed negligible difference in charge before and after the charging process. Environmental changes such as humidity can accelerate the decay of charges* [113].

Results show various charging capabilities in the materials. For example, the 3M6 material (3M 600 MPR) shows one of the largest electrostatic potentials after the charging process. Other materials such as the Honeywell R4 show resistance to any charge storage. Over time only 5 of the materials showed residual charge storage capabilities. In this case two of the 3M brand filters, 3M1000 and 3M2000 showed the largest electrostatic voltage at the end of the study. This suggests they have the best electrostatic filtering capabilities in magnitude and time duration.

A one-hour charging process at a 20kV potential and 5 cm distance was applied to all the materials. **Figure 33** shows the results of measuring the electrostatic surface charge potential of the materials over a twenty-day period. Each material was cut into 1 cm squares. The materials were then placed on the ground electrode of the corona charging system. The voltage supply was set at 20kV for one hour. It is found that 3M6 has superiority in terms

of the electrostatic surface charge potential. Some of the variability may be attributed to experimental error. For the reliability of the result, the experiment should be repeated by taking multiple measurements on multiple locations daily. Additionally, the probing should occur from the exact same height on every sample as this can vary results as well. At the conclusion of the study, it retained near a 1000-volt surface potential after 21 days. The increase from 250V to 1500V suggests clear experimental errors as there is no known mechanism to increase the surface potential to this high level in normal conditions and additional tests are required to get a more consistent charging result. Some materials such as the 3M3 has high initial charge potential but fails to hold the charge over time. Prior research showed that 3M uses a PVDF material which is known for high electrostatic efficiency [114].

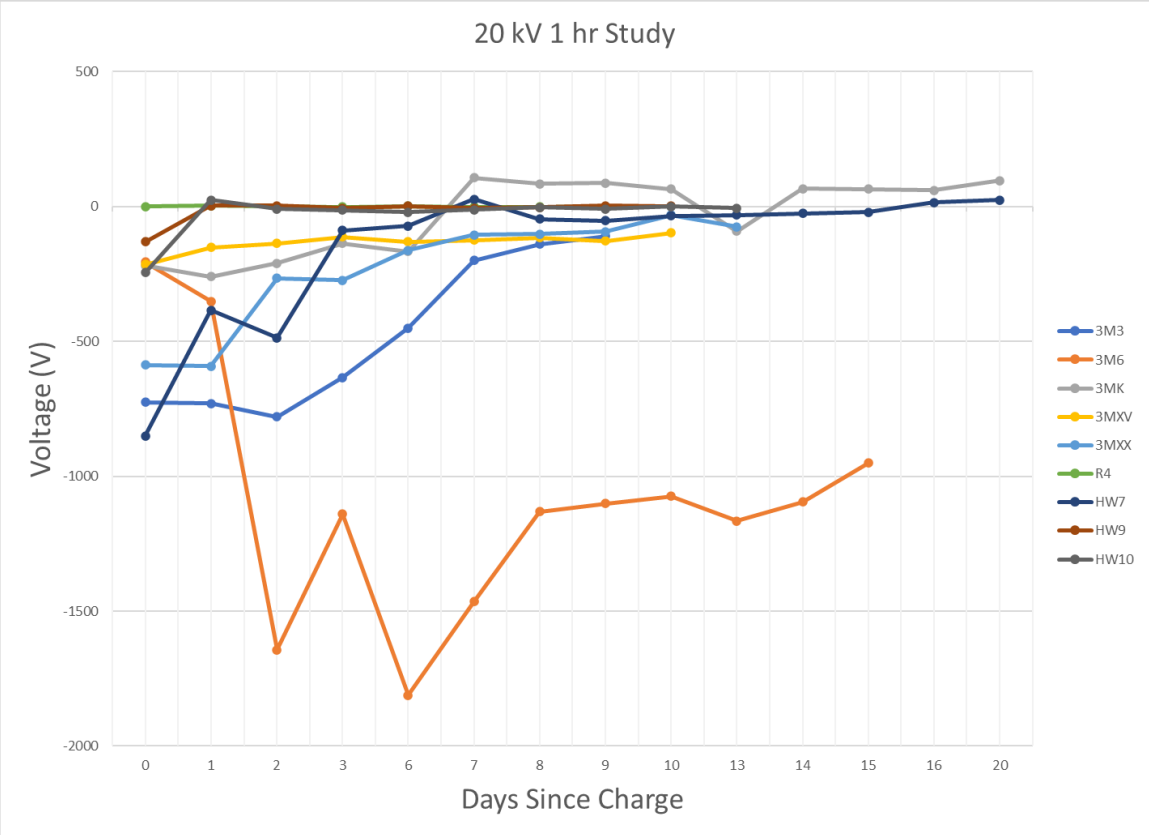


***Figure 32**, 20kV, 1-Hour, and 5 cm distance Corona Charging Study. 3M6 shows superior charge storage as compared to other materials. Environmental factors such as heat and humidity affect the day-to-day variation of charges.*

4.2.3 Further 3M6 Material Studies

The 3M6 material was further studied due to its very high surface potential after the Corona charging process. It was subjected to the charging conditions of 1, 5, and 10kV for one minute to evaluate its charging capabilities. The samples were placed individually on the ground electrode of the corona charging system. The needle tip voltage was set the

prescribed voltage for that experiment. **Figure 34** shows the results of the 1 kV charge process for four samples of the same material. The 3M6 material showed an initial charge of 200V and then increased in charge the following day. This sudden jump is not reasonable as there is no known mechanism for the sudden increase in surface potential under the normal condition and requires repeated measurements in future work. The initial voltage varies among samples especially in comparison to Figure 31. This is attributed to various factors such as changes in humidity, temperature, and sample lifetime.

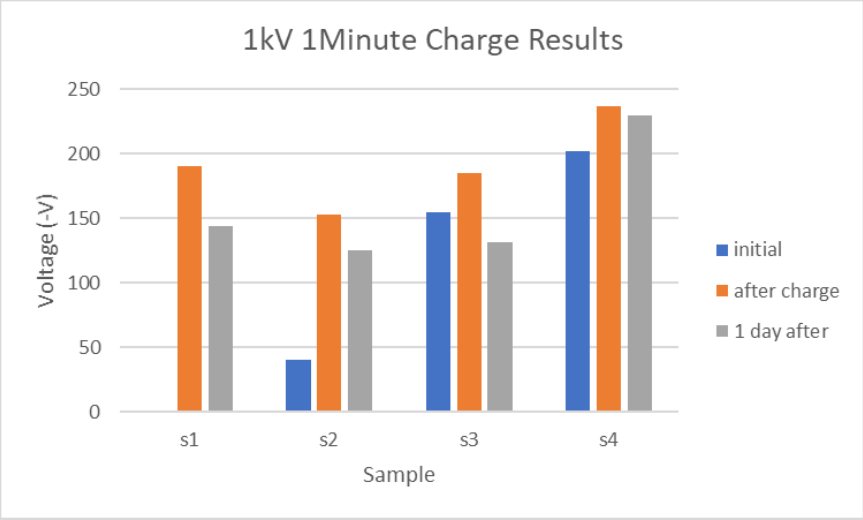


***Figure 33**, 1 kV, 1-Minute Corona Charging Process. Sample s1 shows negligible initial charge potential. Sample s4 shows high initial potential and slight variations after the charging process.*

Results of the initial surface potential measurements show that the material holds varying amounts of charges. After the one-minute charging process, results show that the material can hold more than 200 V of electrostatic potential. Furthermore, after one day storage in the ambient environment, the material can retain a portion of its implanted charges. **Figure 35** shows results of the 10kV charging process for one minute with a 5 cm distance between the corona needle and the sample.

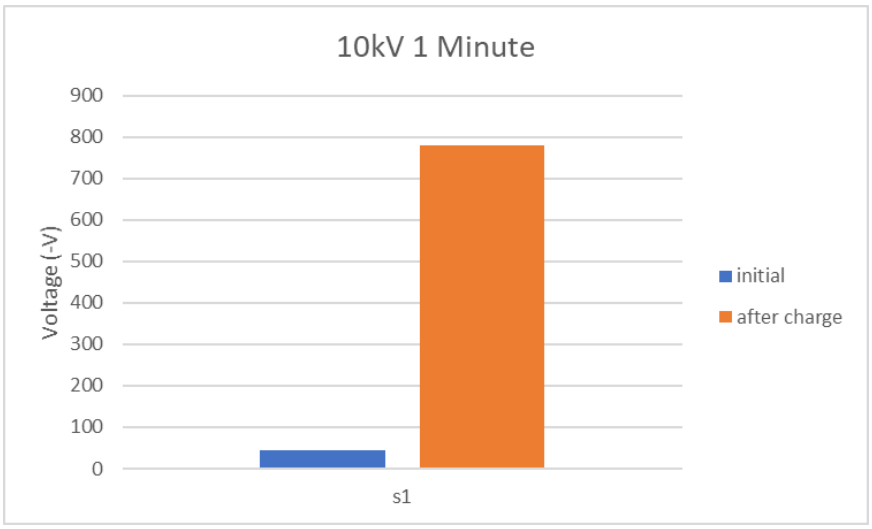


Figure 34, *10kV 1 Minute Charge. The large difference between initial and post processing charge suggests desirable electrostatic charging properties.*

After the charging process, the material shows a surface potential close to 800V. This suggests the material has the good charge storage capability to hold many charges for the high surface potential. **Figure 36** shows the results of charging for one minute, and 5kV, with a 5 cm gap distance.

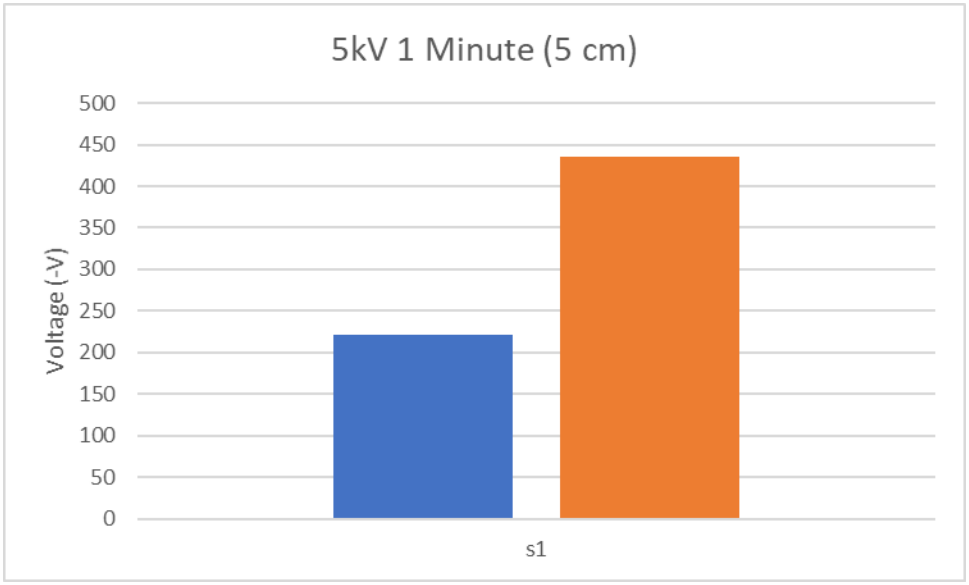


Figure 35*, 5 kV, 1-Minute Corona Charging Process with a 5 cm gap distance.*

The initial charge in blue shows a high surface potential of over 200V as this sample was charged a few days before this new charging process. The results show that the charge can be doubled by applying 5kV for one minute. This charging result further supports the materials as a good electrostatic polymer to hold charges.

The material shows an affinity for charging using the corona charging method. The relationship between a decreasing charging distance and an increasing surface charge will

result in high electrostatic potential for high charge breakdown process for more surface charge storages as documented in many previous studies [115].

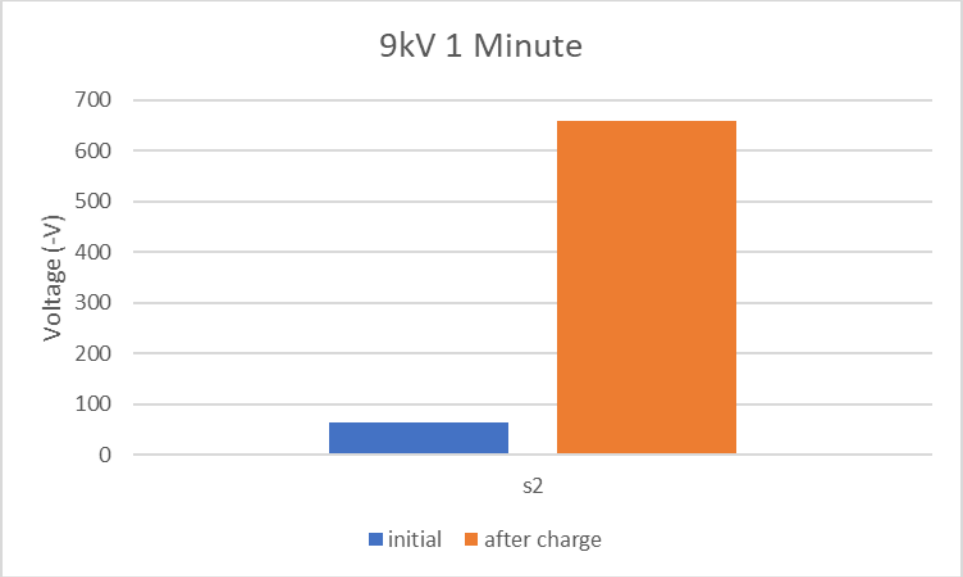


***Figure 36**, 9kV, 1 Minute and 5 cm in distance Charge process. The 9kV charging shows significant charging that is comparable but lower than that of the 10kV result as expected.*

Finally, a 9kV charge for one minute at five-centimeter distance is studied with results shown in **Figure 37**. The material achieves about 10 times the initial charge. In summary, the results show that 3M branded 300MPR has the best electrostatic performance. It can hold charge over the longest period and has the largest surface charge potential. This suggests that this material has the best electrostatic charging capability and thus could potentially filter electrostatic particles like Covid-19 the best. Manufactures could add an electrostatic charging step like the one performed in this study to increase the filtration of their products. This would help reduce the transmission of Covid-19 and other charged airborne particles.

4.3 Case Study: A Generic Air Filter

This case study is part of a Covid-19 project during the spring of the 2020 COVID-19 pandemic funded by CITRIS (Center for Information Technology Research in the Interest of Society) at the University of California, Berkeley with an international collaboration with the Tecnologico de Monterrey, Mexico also known as Tec de Monterrey. Their micro and nanofabrication research group has good experiences in designing and fabricating air filtration prototypes. For this project, it is proposed that a commercially available air filter is combined with a UV light exposure system for Covid-19 particle capture and destruction and **Figure 38** shows the preliminary prototype. A purple-color generic filter from a Chinese manufacturer has been used in the early stage of the project for purifications and UV light has been proposed to destroy viral particles[116][117]. Electrostatically charged filter is proposed to attract and grab viruses as previously discussed. Before widely

available vaccines and other forms of immunity, filtering air from viral particles was seen as the main way to allow people to congregate in enclosed spaces [118], [119].



***Figure 37**, Tec de Monterrey Prototype. The prototype is housed in an acrylic chamber. The chamber is filled with cigarette smoke to assess the filtering performance of the prototype.* [120][116][117][118], [119]

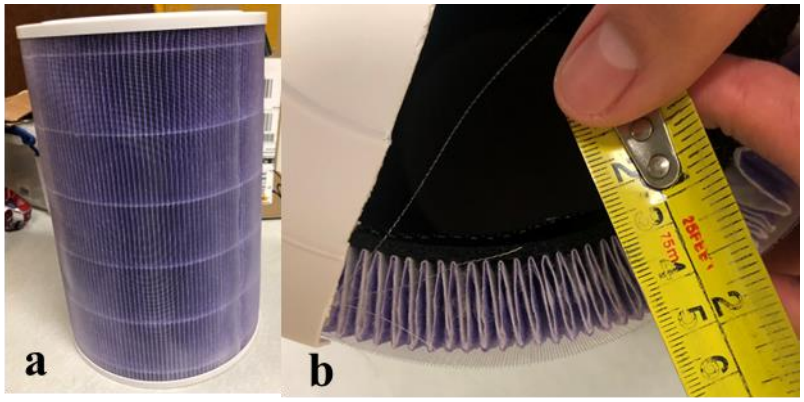


***Figure 39**, Generic Air Filter Photos with Cross Section: (a) the filter standing up; (b) top plastic casing is removed to expose the internal filtering materials.*

A generic commercial filter with advertised electrostatic capabilities was studied for its electrostatic filtering capabilities. **Figure 39a** shows the optical image of the filter. The close-up image in **Figure 39b** shows the layered structure to create a hollow cylinder with

edges. The filter was cut open to access its various layers as shown in **Figure 40**, including: (a) the purple color paper-like filter, (b) white/transparent mesh structure, (c) black metallic wire, and (d) carbon black filter that looks like a sponge. Each material is evaluated for its electrostatic properties.

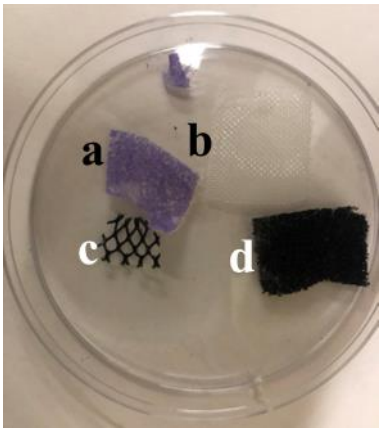


Figure 38, *Generic Air Filter Materials: (a) purple paper-like filter, (b) white/transparent mesh, (c) black metallic wire, (d) carbon black filter that looks like a sponge. Each material is evaluated for its electrostatic properties.*

The carbon sponge layer is advertised as an odor capturing layer. The purple filter layer visually resembles the filter materials discussed in the previous section of commercially available filter materials, suggesting that this is the main filter component. The black metallic wire provides physical structure and the white mesh seems to be the containment of the system. The electrostatic properties of these layers are investigated by cutting these materials into individual samples of one-centimeter squares. Each one has its electrostatic potential measured. After the material is charged using the corona charging process for one-minute at 10kV with a 5cm distance from the corona needle, the surface potentials are measured and results are shown in **Figure 41**.

Results show that the purple air filter and the white mesh material have the highest electrostatic charge potential 225 and 275 V, respectively. The black wire and the carbon sponge show negligible electrostatic charge capability before and after the charging process. The study demonstrates that a generic air filter can be a reasonably good electret material with decent electrostatic charging properties in specific components such as the purple air filter and white mesh material in the case study. However, the carbon sponge and metallic wire can only provide physical filtering and structural support without the electrostatic charging capability. This study also shows that by adding electrostatic charge through the corona charging process can enhance its electrostatic filtering capacity for the capture of Covid-19 viral particles. However, the surface charge potential may degrade overtime. In order to maintain a high surface charge potential, one possible approach is to add an in-situ Corona charging setup with both positive and negative mesh electrodes to boost the surface potential from time to time using the Corona charging process.

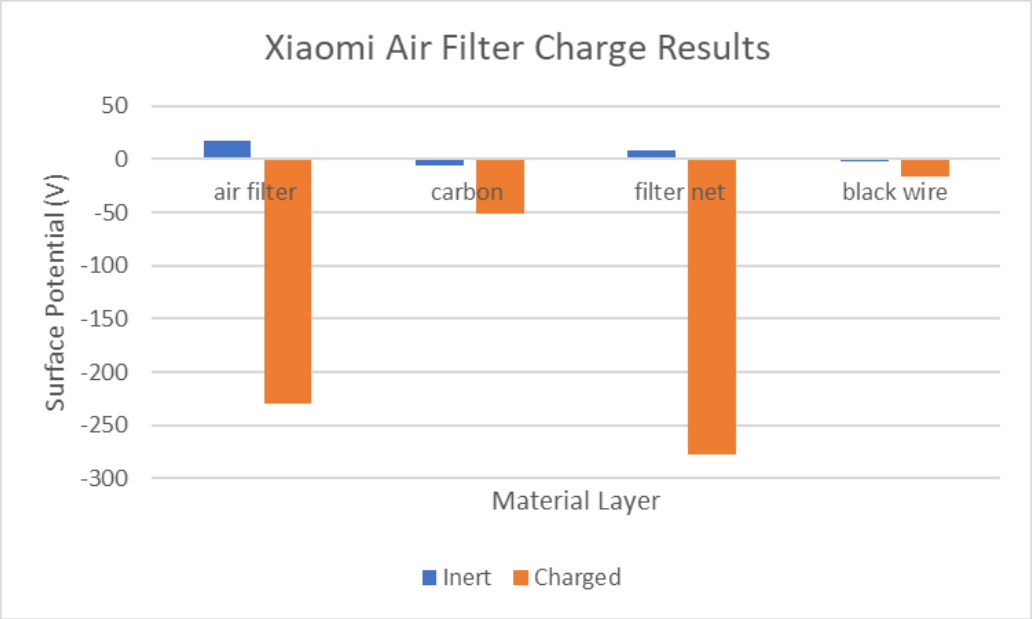


Figure 39, *Generic Air Filter Material Charging Results. The black wire and carbon sponge show low surface charge potentials. The purple air filter shows a high surface charge potential at -230 Volts and the white filter net show a electrostatic surface charge potential at -280 Volts.*

4.4 Air Filtration Conclusions

In summary, there are several conclusions from the study. Firstly, testing results show several commercially advertised electrostatic filters don't have the electrostatic behavior when studied under laboratory conditions. This is important for consumers to know as the advertisement can be used to increase the attractiveness of the product without truly increasing any benefit to the consumer. While some commercial filters do show the electrostatic capability but their surface charge potentials are low as compared to the freshly charged samples enhanced by the corona charging process as brief as one minute. However, the increased surface charge potential decays over time due to the environmental exposure and this effect is difficult to prevent by common packages. It is suggested that filter manufactures could apply these results to identify schemes to increase the efficiencies of their products and ultimately benefit air filtration. One possible approach is to add an in-situ Corona charging setup with both positive and negative mesh electrodes to boost the surface potential from time to time using the Corona charging process. With better performing filters based on enhanced electrostatic properties, dangerous particulates such as Covid-19 could be better filtered.

5 Conclusions and Future Work

5.1 Electrostatic Polymers for Energy Harvesters

This work demonstrates the design, fabrication, characterization, and application of electrostatic polymers for energy harvesters. A FEP-based stack structure can be charged with the Corona charging process. By constructing a sandwich structure and connecting the device to an external circuit, a prototype device can produce electricity by subjecting it to compressive forces. The output voltages are capable of powering LEDs and other electronics. Under ultrasonic vibrations in water, the mechanical energy can deform the device to result in electrical potential large enough for the electrolysis process to generate Hydrogen, which is characterized by GC measurements.

The development of an electrostatic polymer device using biodegradable materials is presented. The biodegradable materials are PLA, cellulose paper, and PEDOT: PSS. By combining the materials in a sandwich structure, a biodegradable energy harvesting device is fabricated. The device shows output voltages capable of powering an LED. A ceramic piezoelectret device is proposed for high charge storage capabilities. The key material tested is SiO_2 and the preliminary work shows little promise due to the complications in material compatibility.

5.2 Electrostatic polymers for air filtration

Covid-19 increased worldwide interest in air filtration technologies. This work studies commercial air filters and their claims of using electrostatic technology in their products. Few products show the capability to store charges after the Corona charging process during studies. Furthermore, the charge storage capability can be enhanced through the corona charging process from time to time and repetitively. This increases the amount of charge they can hold over time and their efficacy at filtering Covid-19 particles. In addition, a commercially available air filter was studied to evaluate its electrostatic properties in collaboration with Tec de Monterrey. Studies showed that some layers in the product had electrostatic properties as they showed that the electrostatic charge could be increased using the corona charging process.

5.3 Future Work

Future works include the optimization of polymers used in this study for their respective applications. Based on the mathematical theory of piezoelectrets, a compromise must be made between decreasing the cross-sectional area and increasing the amount of area available to impart charges during the corona charging process. Additional work can be done to prescribe a manufacturing process that will yield cellulose paper that can provide structure supports for PLA and PEDOT: PSS in the biodegradable energy harvester. This device then can be studied for its biodegradable efficacy. Tests for its degradation under composting environment should be conducted. For the hydrogen production energy harvesting, much work remains to be done to investigate the efficiency of the conversion

process as there are many more gas chromatography measurements to be made to assess the amount of energy conversion efficiencies. There is a lot of further studies to be done in terms of the ultrasonic inputs as well.

In the air filtration work, more studies should be done to characterize the amount of charges that is present in materials. Long term studies that span the same amount of time as typical air filter use should be conducted to determine the efficacy of the materials. In addition, the materials should be subjected to measurements regarding the actual filtration of particles. Using a Phase Doppler Interferometer would complete the scope of this study by measuring how many particles can pass through the electrostatic filters during operations. It would also be interesting to alter the charging method for the materials in addition to the Corona charging method, such as the pyroelectric charging method, which could potentially increase the efficiency for certain devices.

Bibliography

[1] S. Alavi, S. Thomas, K. P. Sandeep, N. Kalarikkal, J. Varghese, and S. Yaragalla, *Polymers for Packaging Applications*. Toronto, New Jersey: Apple Academic Press, 2015. [Online]. Available: https://books.google.com/books?hl=en&lr=&id=9QRZBAAAQBAJ&oi=fnd&pg=PP1&dq=food+packaging+polymers&ots=Nh0i6EYYWb&sig=LdeuCGz5Tk30_wMm05hMQxQFXag#v=onepage&q=food packaging polymers&f=false

[2] P. P. Tsai, W. Chen, and J. R. Roth, "Investigation of the Fiber, Bulk, and Surface Properties of Meltblown and Electrospun Polymeric Fabrics," *International Nonwovens Journal*, vol. os-13, no. 3, pp. 1558925004os–13, 2004, doi: 10.1177/1558925004os-1300306.

[3] J. Price, "The effect of high-intensity solid polymers," *Science (1979)*, vol. 36, no. 26, pp. 4919–4925, 1995.

[4] G. M. Sessler, "Electrets : recent developments," vol. 52, pp. 137–145, 2001.

[5] H. J. Peng, J. Q. Huang, and Q. Zhang, "A review of flexible lithium-sulfur and analogous alkali metal-chalcogen rechargeable batteries," *Chem Soc Rev*, vol. 46, no. 17, pp. 5237–5288, 2017, doi: 10.1039/c7cs00139h.

[6] O. Mellbring, S. K. Øiseth, A. Krozer, J. Lausmaa, and T. Hjertberg, "Spin coating and characterization of thin high-density polyethylene films," *Macromolecules*, vol. 34, no. 21, pp. 7496–7503, 2001, doi: 10.1021/ma000094x.

[7] J. Zhong, H. Zhu, Q. Zhong, J. Dai, and W. Li, "Self-Powered Human Interactive Transparent Nanopaper Systems Self-Powered Human Interactive Transparent Nanopaper Systems," *ACS Nano*, no. 7, pp. 7399–7406, 2015, doi: 10.1021/acsnano.5b02414.

[8] J. Zhong *et al.*, "Flexible PET/EVA-based piezoelectret generator for energy harvesting in harsh environments," *Nano Energy*, vol. 37, pp. 268–274, 2017, doi: 10.1016/j.nanoen.2017.05.034.

[9] E. G. M. Sessler, R. G. B. G. S. Mascarenhas, and G. M. S. J. V. T. J. E. West, *Electrets*.

[10] J. Zhong *et al.*, "Flexible PET/EVA-based piezoelectret generator for energy harvesting in harsh environments," *Nano Energy*, vol. 37, pp. 268–274, 2017, doi: 10.1016/j.nanoen.2017.05.034.

[11] T. H. Kim, "Characterization and applications of piezoelectric polymers," *Thesis of Master*, p. 29, 2015, [Online]. Available: http://www.eecs.berkeley.edu/Pubs/TechRpts/2015/EECS-2015-253.html

[12] S. P. Beeby, M. J. Tudor, and N. M. White, “Energy harvesting vibration sources for microsystems applications,” *Meas Sci Technol*, vol. 17, no. 12, 2006, doi: 10.1088/0957-0233/17/12/R01.

[13] Q. Sun and W. W. F. Leung, “Charged PVDF multi-layer filters with enhanced filtration performance for filtering nano-aerosols,” *Sep Purif Technol*, vol. 212, pp. 854–876, 2019, doi: 10.1016/j.seppur.2018.11.063.

[14] A. Bartholomeusz and S. Locarnini, “Exhalation of Respiratory Viruses by Breathing, Coughing, and Talking,” *J Med Virol*, vol. 55, no. November 2005, pp. 52–55, 2006, doi: 10.1002/jmv.

[15] N. H. L. Leung *et al.*, “Respiratory virus shedding in exhaled breath and efficacy of face masks,” *Nat Med*, vol. 26, no. May, 2020, doi: 10.1038/s41591-020-0843-2.

[16] H. Liu, J. Zhong, C. Lee, S. W. Lee, and L. Lin, “A comprehensive review on piezoelectric energy harvesting technology: Materials, mechanisms, and applications,” *Applied Physics Reviews*, vol. 5, no. 4. American Institute of Physics Inc., Dec. 01, 2018. doi: 10.1063/1.5074184.

[17] Q. Sun and W. W. Leung, “Enhanced nano-aerosol loading performance of multilayer PVDF nanofiber electret filter,” *Sep Purif Technol*, no. January, 2020.

[18] A. L. Ahmad, W. K. W. Ramli, W. J. N. Fernando, and W. R. W. Daud, “Effect of ethanol concentration in water coagulation bath on pore geometry of PVDF membrane for Membrane Gas Absorption application in CO2removal,” *Sep Purif Technol*, vol. 88, pp. 11–18, 2012, doi: 10.1016/j.seppur.2011.11.035.

[19] Y. Qiu, K. Yan, H. Deng, and S. Yang, “Secondary branching and nitrogen doping of ZnO nanotetrapods: Building a highly active network for photoelectrochemical water splitting,” *Nano Lett*, vol. 12, no. 1, pp. 407–413, 2012, doi: 10.1021/nl2037326.

[20] T. R. Shrout and S. J. Zhang, “Lead-free piezoelectric ceramics : Alternatives for PZT ?,” no. September 2006, pp. 111–124, 2007, doi: 10.1007/s10832-007-9047-0.

[21] X. Yang *et al.*, “Nitrogen-Doped ZnO Nanowire Arrays for Photoelectrochemical Water Splitting,” *Nano Lett*, vol. 9, no. 6, pp. 2331–2336, 2009, doi: 10.1021/nl900772q.

[22] Y. Wang, Y. Yang, and Z. L. Wang, “Triboelectric nanogenerators as flexible power sources,” *npj Flexible Electronics*, vol. 1, no. 1, pp. 1–9, 2017, doi: 10.1038/s41528-017-0007-8.

[23] F. R. Fan, Z. Q. Tian, and Z. Lin Wang, “Flexible triboelectric generator,” *Nano Energy*, vol. 1, no. 2, pp. 328–334, 2012, doi: 10.1016/j.nanoen.2012.01.004.

[24] M. (Cambridge U. Ashby, “Material and Process Charts,” 2010.

[25] J. Zhong *et al.*, “Finger typing driven triboelectric nanogenerator and its use for instantaneously lighting up LEDs,” *Nano Energy*, vol. 2, no. 4, pp. 491–497, 2013, doi: 10.1016/j.nanoen.2012.11.015.

[26] W. N. Sharpe, B. Yuan, R. Vaidyanathan, and R. L. Edwards, “Measurements of Young ’ S Modulus , Poisson ’ S Ratio , and Tensile Strength of Polysilicon,” *Proceedings of the Tenth IEEE International Workshop on Microelectromechanical Systems*, vol. 429, pp. 424–429, 1997, doi: 10.1109/MEMSYS.1997.581881.

[27] J. Zhong *et al.*, “Finger typing driven triboelectric nanogenerator and its use for instantaneously lighting up LEDs,” *Nano Energy*, vol. 2, no. 4, pp. 491–497, 2013, doi: 10.1016/j.nanoen.2012.11.015.

[28] Y. Chu *et al.*, “Human Pulse Diagnosis for Medical Assessments Using a Wearable Piezoelectret Sensing System,” *Adv Funct Mater*, vol. 28, no. 40, pp. 1–10, 2018, doi: 10.1002/adfm.201803413.

[29] W. Tang, Y. Han, C. B. Han, C. Z. Gao, X. Cao, and Z. L. Wang, “Self-powered water splitting using flowing kinetic energy,” *Advanced Materials*, vol. 27, no. 2, pp. 272–276, 2015, doi: 10.1002/adma.201404071.

[30] H. Guo *et al.*, “A nanogenerator for harvesting airflow energy and light energy,” *J Mater Chem A Mater*, vol. 2, no. 7, pp. 2079–2087, 2014, doi: 10.1039/c3ta14421f.

[31] A. Khaligh, S. Member, P. Zeng, S. Member, C. Zheng, and S. Member, “Kinetic Energy Harvesting Using Piezoelectric and Electromagnetic Techniques - State of the Art,” vol. 57, no. 3, pp. 850–860, 2010, doi: 10.1109/TIE.2009.2024652.

[32] Z. Liu, M. Zeng, H. Wang, X. Wang, Y. Li, and C. Zeng, “Toward Flexible Piezoelectrets with High Environmental Stability: A Hybrid Approach,” *ES Materials & Manufacturing*, 2022, doi: 10.30919/ESMM5F631.

[33] R. Pinto, P. Gonzalez-Losada, M. Faraji, and K. B. Vinayakumar, “Pyroelectrically-Charged Flexible Piezoelectret Sensors: Route Towards Sustainable Functional Electronics,” *IEEE Symposium on Mass Storage Systems and Technologies*, vol. 2022-January, pp. 547–550, 2022, doi: 10.1109/MEMS51670.2022.9699473.

[34] L. Han *et al.*, “Mapping and Simultaneous Detection of Arterial and Venous Pulses using Large-Scale High-Density Flexible Piezoelectret Sensor Array,” *Adv Electron Mater*, p. 2200012, 2022, doi: 10.1002/AELM.202200012.

[35] W. Li *et al.*, “Theoretical Study of Cellular Piezoelectret Generators,” *Adv Funct Mater*, vol. 26, no. 12, pp. 1964–1974, Mar. 2016, doi: 10.1002/adfm.201503704.

[36] L. Ekstam, “Capacitor Theory,” *IEEE Transactions on Dielectrics and Electrical Insulation*, vol. 1, no. 5, pp. 826–839, 1994, doi: 10.1109/94.326654.

[37] N. Chouhan, R.-S. Liu, and J. Zhang, *Photochemical Water Splitting*. 2017. doi: 10.1201/9781315279657.

[38] S. Priya and D. J. Inman, *Energy Harvesting Technologies*. Springer, 2009. doi: 10.1007/978-0-387-76464-1.

[39] I. Dincer, “Environmental issues: I-energy utilization,” *Energy Sources*, vol. 23, no. 1, pp. 69–81, 2001, doi: 10.1080/00908310151092191.

[40] C.-J. Winter and J. Nitsch, *Hydrogen as an Energy Carrier*, vol. 1, no. 11. Springer-Verlag, 1988.

[41] S. B. Sheavly and K. M. Register, “Marine Debris & Plastics: Environmental Concerns, Sources, Impacts and Solutions,” *J Polym Environ*, vol. 15, no. 4, pp. 301–305, 2007, doi: 10.1007/s10924-007-0074-3.

[42] Nakamura, B.J., S. R. Narayanan, T. I. Valdez, and W. Chun, “Making hydrogen by electrolysis of methanol: NASA Tech Brief,” pp. 5–7, 1948.

[43] N. Khan, A. Kalair, N. Abas, and A. Haider, “Review of ocean tidal, wave and thermal energy technologies,” *Renewable and Sustainable Energy Reviews*, vol. 72, no. January, pp. 590–604, 2017, doi: 10.1016/j.rser.2017.01.079.

[44] N. Mallos, A. Schutes, and A. Williams, “Ocean Conservancy Annual Report,” 2015.

[45] M. Science, “Energy harvesting vibration sources for microsystems applications,” 2006, doi: 10.1088/0957-0233/17/12/R01.

[46] Y. Zhang, M. Xie, V. Adamaki, H. Khanbareh, and C. R. Bowen, “Control of electro-chemical processes using energy harvesting materials and devices,” *Chem Soc Rev*, vol. 46, pp. 7757–7786, 2017, doi: 10.1039/C7CS00387K.

[47] W. L. Guo, L. Li, L. L. Li, S. Tian, S. L. Liu, and Y. P. Wu, “Hydrogen production via electrolysis of aqueous formic acid solutions,” *Int J Hydrogen Energy*, vol. 36, no. 16, pp. 9415–9419, 2011, doi: 10.1016/j.ijhydene.2011.04.127.

[48] D. Zhang and K. Zeng, “Evaluating the behavior of electrolytic gas bubbles and their effect on the cell voltage in alkaline water electrolysis,” *Ind Eng Chem Res*, vol. 51, no. 42, pp. 13825–13832, 2012, doi: 10.1021/ie301029e.

[49] A. Fujishima and K. Honda, “Electrochemical photolysis of water at a semiconductor electrode,” *Nature*, vol. 238, no. 5358, pp. 37–38, 1972, doi: 10.1038/238037a0.

[50] M. Wegener and S. Bauer, “Microstorms in cellular polymers: A route to soft piezoelectric transducer materials with engineered macroscopic dipoles,”

ChemPhysChem, vol. 6, no. 6, pp. 1014–1025, 2005, doi: 10.1002/cphc.200400517.

[51] P. Fang *et al.*, “Piezoelectrets and their applications as wearable physiological-signal sensors and energy harvesters,” *2015 IEEE 12th International Conference on Wearable and Implantable Body Sensor Networks, BSN 2015*, 2015, doi: 10.1109/BSN.2015.7299373.

[52] S. Fedosov and M. M. Costa, “Corona Charging of Polymers Recent Advances,” vol. 29, no. 2, 1999.

[53] S. Dangeam, “A Design of single phase induction generator for waterfall-hydro turbine,” *Energy Procedia*, vol. 34. pp. 130–141, 2013. doi: 10.1016/j.egypro.2013.06.741.

[54] V. Morosini, T. Chave, M. Virot, P. Moisy, and S. I. Nikitenko, “Sonochemical water splitting in the presence of powdered metal oxides,” *Ultrason Sonochem*, vol. 29, pp. 512–516, 2016, doi: 10.1016/j.ultsonch.2015.11.006.

[55] V. Morosini, T. Chave, M. Virot, P. Moisy, and S. I. Nikitenko, “Sonochemical water splitting in the presence of powdered metal oxides,” *Ultrason Sonochem*, vol. 29, pp. 512–516, 2016, doi: 10.1016/j.ultsonch.2015.11.006.

[56] J. Gong, J. Liang, and K. Sumathy, “Review on dye-sensitized solar cells (DSSCs): Fundamental concepts and novel materials Renewable and Sustainable Energy Reviews,” *Energy Reviews*, vol. 16, pp. 5848–5860, 2012.

[57] I. Martínez de Alegría, I. Kortabarria, J. Andreu, I. López, and S. Ceballos, “Review of wave energy technologies and the necessary power-equipment,” *Renewable and Sustainable Energy Reviews*, vol. 27. pp. 413–434, 2013. doi: 10.1016/j.rser.2013.07.009.

[58] B. Wang *et al.*, “Sandwiched Composite Fluorocarbon Film for Flexible Electret Generator,” *Adv Electron Mater*, vol. 2, no. 4, pp. 1–6, 2016, doi: 10.1002/aelm.201500408.

[59] A. Bouteffaha, A. Bendaoud, A. Reguig, and L. Dascalescu, “Effects of the grid geometry on the performances of a triode-type corona electrode system,” *J Electrostat*, vol. 101, no. June, p. 103367, 2019, doi: 10.1016/j.elstat.2019.103367.

[60] L. Hu *et al.*, “Highly conductive paper for energy-storage devices,” *Proceedings of the National Academy of Sciences*, vol. 106, no. 51, pp. 21490–21494, 2009, doi: 10.1073/pnas.0908858106.

[61] E. Insulation, “Mechanism of Charge Storage,” vol. 26, no. 1, pp. 42–48, 1991.

[62] C. A. Grimes, O. K. Varghese, and S. Ranjan, *Light, water, hydrogen: The solar generation of hydrogen by water photoelectrolysis*. 2008. doi: 10.1007/978-0-387-68238-9.

[63] L. Liao *et al.*, “Efficient solar water-splitting using a nanocrystalline CoO photocatalyst,” *Nat Nanotechnol*, vol. 9, no. 1, pp. 69–73, 2014, doi: 10.1038/nnano.2013.272.

[64] L. Cited, “Determination of Methyltin (IV) and Tin (IV) Species in Water by Gas Chromatography / Atomic Absorption Spectrophotometry,” vol. 249, no. 9, pp. 246–249, 1982.

[65] J. A. Malecki, “Linear decay of charge in electrets,” *Phys Rev B*, vol. 59, no. 15, pp. 9954–9960, 1999.

[66] H. T. Baytekin, A. Z. Patashinski, M. Branicki, S. Soh, and B. a. Grzybowski, “The Mosaic of Surface Charge in,” vol. 333, no. July, pp. 308–313, 2011, doi: 10.1126/science.1201512.

[67] M. Liu, C. Nam, C. T. Black, J. Kamcev, and L. Zhang, “Enhancing Water Splitting Activity and Chemical Stability of Zinc Oxide Nanowire Photoanodes with Ultrathin Titania Shells,” 2013, doi: 10.1021/jp404032p.

[68] G. D. Berry, “Hydrogen Production,” vol. 3, pp. 253–265, 2004, doi: http://dx.doi.org/10.1016/B0-12-176480-X/00350-8.

[69] T. P. Cell, *Photoelectrochemical Hydrogen Production*, vol. 102. 2012. doi: 10.1007/978-1-4614-1380-6.

[70] R. van de Krol and M. Gr, “Photoelectrochemical Hydrogen Production,” vol. 102, pp. 3–11, 2012, doi: 10.1007/978-1-4614-1380-6.

[71] K. Mazloomi, N. B. Sulaiman, and H. Moayedi, “Electrical efficiency of electrolytic hydrogen production,” *Int J Electrochem Sci*, vol. 7, no. 4, pp. 3314–3326, 2012.

[72] K. Marsh and B. Bugusu, “Food packaging - Roles, materials, and environmental issues: Scientific status summary,” *J Food Sci*, vol. 72, no. 3, 2007, doi: 10.1111/j.1750-3841.2007.00301.x.

[73] R. Geyer, J. R. Jambeck, and K. L. Law, “Production, use, and fate of all plastics ever made,” *Sci Adv*, vol. 3, no. 7, p. e1700782, Jul. 2017, doi: 10.1126/sciadv.1700782.

[74] S. Bauer, R. Gerhard-Multhaupt, and G. M. Sessler, “Ferroelectrets: Soft Electroactive Foams for Transducers,” *Phys Today*, vol. 57, no. 2, pp. 37–43, 2004, doi: 10.1063/1.1688068.

[75] M. Yang, Y. Zhang, H. Zhang, and Z. Li, “Characterization of PEDOT : PSS as a Biocompatible Conductive Material,” pp. 149–151, 2015.

[76] C. Duc, A. Vlandas, G. G. Malliaras, and V. Senez, “Wettability of PEDOT:PSS films,” *Soft Matter*, vol. 12, no. 23, pp. 5146–5153, 2016, doi: 10.1039/c6sm00599c.

[77] I. S. Bayer *et al.*, “Water-repellent cellulose fiber networks with multifunctional properties,” *ACS Appl Mater Interfaces*, vol. 3, no. 10, pp. 4024–4031, 2011, doi: 10.1021/am200891f.

[78] M. Nogi, C. Kim, T. Sugahara, T. Inui, T. Takahashi, and K. Suganuma, “High thermal stability of optical transparency in cellulose nanofiber paper,” *Appl Phys Lett*, vol. 102, no. 18, 2013, doi: 10.1063/1.4804361.

[79] H. Koga, M. Nogi, N. Komoda, T. T. Nge, T. Sugahara, and K. Suganuma, “Uniformly connected conductive networks on cellulose nanofiber paper for transparent paper electronics,” *NPG Asia Mater*, vol. 6, no. 3, pp. e93-8, 2014, doi: 10.1038/am.2014.9.

[80] X. Gao *et al.*, “Natural Materials Assembled, Biodegradable, and Transparent Paper-Based Electret Nanogenerator,” *ACS Appl Mater Interfaces*, vol. 8, no. 51, pp. 35587–35592, 2016, doi: 10.1021/acsami.6b12913.

[81] M. C. Hsieh, C. Kim, M. Nogi, and K. Suganuma, “Electrically conductive lines on cellulose nanopaper for flexible electrical devices,” *Nanoscale*, vol. 5, no. 19, pp. 9289–9295, 2013, doi: 10.1039/c3nr01951a.

[82] S. Sato, D. Gondo, T. Wada, S. Kanehashi, and K. Nagai, “Effects of various liquid organic solvents on solvent-induced crystallization of amorphous poly(lactic acid) film,” *J Appl Polym Sci*, vol. 129, no. 3, pp. 1607–1617, 2013, doi: 10.1002/app.38833.

[83] E. Vismara, G. Gastaldi, A. Valerio, S. Bertini, C. Cosentino, and G. Eisle, “Alpha cellulose from industrial and agricultural renewable sources like short flax fibres, ears of corn and wheat-straw and its transformation into cellulose acetates,” *J Mater Chem*, vol. 19, no. 45, pp. 8678–8686, 2009, doi: 10.1039/b911610a.

[84] Y. Mao, L. Zhang, J. Cai, J. Zhou, and T. Kondo, “Multifilament Fibers Based on Dissolution of Cellulose in NaOH/Urea Aqueous Solution: Structure and Properties,” *Ind Eng Chem Res*, vol. 47, no. 22, pp. 8676–8683, 2008, doi: 10.1021/ie800833w.

[85] M. Jamshidian, E. A. Tehrany, M. Imran, M. Jacquot, and S. Desobry, “Poly-Lactic Acid: Production, applications, nanocomposites, and release studies,” *Compr Rev Food Sci Food Saf*, vol. 9, no. 5, pp. 552–571, 2010, doi: 10.1111/j.1541-4337.2010.00126.x.

[86] X. Guan, “Fabrication of Poly-Lactic Acid (PLA) Composite Films and Their Degradation Properties,” 2012, [Online]. Available: http://rave.ohiolink.edu/etdc/view?acc_num=toledo1333779869

[87] H. Sawada, Y. Takahashi, S. Miyata, S. Kanehashi, S. Sato, and K. Nagai, “Gas Transport Properties and Crystalline Structures of Poly(lactic acid) Membranes,” *Transactions of the Materials Research Society of Japan*, vol. 35, no. 2, pp. 241–246, 2010, doi: 10.14723/tmrsj.35.241.

[88] P. Deejam and S. Charuchinda, “Mechanical properties of poly(lactic acid) sheet reinforced with microfibrillated cellulose from corn cobs,” *MATEC Web of Conferences*, vol. 30, 2015, doi: 10.1051/matecconf/20153003007.

[89] A. Rice and S. Hay, “Measuring mobile phone energy consumption for 802.11 wireless networking,” *Pervasive and Mobile Computing*, vol. 6, no. 6. pp. 593–606, 2010. doi: 10.1016/j.pmcj.2010.07.005.

[90] Y. Shimizu, M. Mizoshiri, M. Mikami, Y. Ito, J. Sakurai, and S. Hata, “Fabrication of flexible thermoelectric generators with a lens array for near-infrared solar light harvesting,” no. January, pp. 604–607, 2018.

[91] Y. Kim *et al.*, “Remote epitaxy through graphene enables two-dimensional material-based layer transfer,” *Nature*, vol. 544, no. 7650, pp. 340–343, 2017, doi: 10.1038/nature22053.

[92] K. Misawa, T. Sugiyama, G. Hashiguchi, and H. Toshiyoshi, “Reliability of potassium ion electret in silicon oxide for vibrational energy harvester applications,” *Jpn J Appl Phys*, vol. 54, no. 6, p. 67201, Apr. 2015, doi: 10.7567/JJAP.54.067201.

[93] W. Olthius and P. Bergveld, “On the charge storage and decay mechanism in silicon dioxide,” *Ieee*, vol. 27, no. 4, 1991, [Online]. Available: http://doc.utwente.nl/15307/1/00155784.pdf

[94] H. W. Lo and Y. C. Tai, “Parylene-based electret power generators,” *Journal of Micromechanics and Microengineering*, vol. 18, no. 10, Oct. 2008, doi: 10.1088/0960-1317/18/10/104006.

[95] Y. Suzuki and Y. C. Tai, “Micromachined high-aspect-ratio parylene spring and its application to low-frequency accelerometers,” *Journal of Microelectromechanical Systems*, vol. 15, no. 5, pp. 1364–1370, Oct. 2006, doi: 10.1109/JMEMS.2006.879706.

[96] J. Boland, Y.-H. Chao, Y. Suzuki, and Y. C. Tai, “Micro electret power generator,” in *The Sixteenth Annual International Conference on Micro Electro Mechanical Systems, 2003. MEMS-03 Kyoto. IEEE*, 2003, pp. 538–541. doi: 10.1109/MEMSYS.2003.1189805.

[97] L. G. Meiners, “ Electrical properties of SiO 2 and Si 3 N 4 dielectric layers on InP ,” *Journal of Vacuum Science and Technology*, vol. 19, no. 3, pp. 373–379, 2002, doi: 10.1116/1.571066.

[98] S. Sasaki, T. Izumi, and T. Hara, “Delamination of Si by high dose H-ion implantation through thin SiO2 film (ESR characterization),” *Mater Sci Eng B Solid State Mater Adv Technol*, vol. 91–92, pp. 160–163, 2002, doi: 10.1016/S0921-5107(01)00984-9.

[99] N. Nagasima, “Structure analysis of silicon dioxide films formed by oxidation of silane,” *J Appl Phys*, vol. 43, no. 8, pp. 3378–3386, 1972, doi: 10.1063/1.1661723.

[100] A. J. Sprenkels, W. Olthuis, and P. Berveld, “The application of silicon dioxide as an electret material,” pp. 165–169, 2003, doi: 10.1109/ise.1988.38543.

[101] T. C. Kho, S. C. Baker-Finch, and K. R. McIntosh, “The study of thermal silicon dioxide electrets formed by corona discharge and rapid-thermal annealing,” *J Appl Phys*, vol. 109, no. 5, 2011, doi: 10.1063/1.3559260.

[102] Z. Feng and S. J. Cao, “A newly developed electrostatic enhanced pleated air filters towards the improvement of energy and filtration efficiency,” *Sustain Cities Soc*, vol. 49, no. April, p. 101569, 2019, doi: 10.1016/j.scs.2019.101569.

[103] M. Zhao *et al.*, “Household Materials Selection for Homemade Cloth Face Coverings and Their Filtration E ffi ciency Enhancement with Triboelectric Charging,” 2020, doi: 10.1021/acs.nanolett.0c02211.

[104] D. Japuntich and N. MCullough, “Respirator that includes an integral filter element, an exhalation valve, and an impactor element,” United States Patent 6460539B1, 2002

[105] W. W. F. Leung and S. Qiangqiang, “Electrostatic Charged Nanofiber Filter for Filtering Airborne Novel Coronavi- rus (COVID-19) and Nano-aerosols,” *Sep Purif Technol*, no. February, 2020.

[106] D. Y. Choi *et al.*, “Al-Coated Conductive Fiber Filters for High-Efficiency Electrostatic Filtration: Effects of Electrical and Fiber Structural Properties,” *Sci Rep*, vol. 8, no. 1, pp. 1–10, 2018, doi: 10.1038/s41598-018-23960-9.

[107] D. Sun, C. Chang, S. Li, and L. Lin, “Near-Field Electrospinning,” 2006.

[108] J. Xue, T. Wu, Y. Dai, and Y. Xia, “Electrospinning and electrospun nanofibers: Methods, materials, and applications,” *Chem Rev*, vol. 119, no. 8, pp. 5298–5415, 2019, doi: 10.1021/acs.chemrev.8b00593.

[109] J. Hong and H. S. Park, “Fabrication and characterization of block copolymer micelle multilayer films prepared using dip-, spin- and spray-assisted layer-by-layer assembly deposition,” *Colloids Surf A Physicochem Eng Asp*, vol. 381, no. 1–3, pp. 7–12, 2011, doi: 10.1016/j.colsurfa.2011.02.014.

[110] Y. J. Hou, K. Okuda, C. E. Edwards, S. H. Randell, R. C. Boucher, and R. S. Baric, “Article SARS-CoV-2 Reverse Genetics Reveals a Variable Infection Gradient in the Respiratory Tract Article SARS-CoV-2 Reverse Genetics Reveals

a Variable Infection Gradient in the Respiratory Tract," pp. 1–18, 2020, doi: 10.1016/j.cell.2020.05.042.

[111] Google, "Commercial Air Filter Images."

[112] P. Basset, E. Blokhina, D. Galayko, P. Basset, E. Blokhina, and D. Galayko, "Introduction to Electrostatic Kinetic Energy Harvesting," *Electrostatic Kinetic Energy Harvesting*, pp. 1–6, 2016, doi: 10.1002/9781119007487.ch1.

[113] C. Liu, Z. Dai, and Q.-F. Ke, "The Effect of Temperature and Humidity on the Filtration Performance of Electret Melt-Blown Nonwovens", doi: 10.3390/ma13214774.

[114] S. P. Deshmukh and K. Li, "Effect of ethanol composition in water coagulation bath on morphology of PVDF hollow fiber membranes," *J Memb Sci*, vol. 150, no. 1, pp. 75–85, 1998, doi: 10.1016/S0376-7388(98)00196-3.

[115] W. Li, N. Wu, J. Zhong, Q. Zhong, S. Zhao, and B. Wang, "Theoretical Study of Cellular Piezoelectret Generators," pp. 1964–1974, 2016, doi: 10.1002/adfm.201503704.

[116] A. Kumar, A. Sagdeo, and P. R. Sagdeo, "Possibility of using ultraviolet radiation for disinfecting the novel COVID-19," *Photodiagnosis Photodyn Ther*, vol. 34, Jun. 2021, doi: 10.1016/j.pdpdt.2021.102234.

[117] K. N. Huynh, B. G. Oliver, S. Stelzer, W. D. Rawlinson, and E. R. Tovey, "A New Method for Sampling and Detection of Exhaled Respiratory Virus Aerosols," *Clinical Infectious Diseases*, vol. 46, no. 1, pp. 93–95, 2008, doi: 10.1086/523000.

[118] M. Raeiszadeh and B. Adeli, "A Critical Review on Ultraviolet Disinfection Systems against COVID-19 Outbreak: Applicability, Validation, and Safety Considerations," *ACS Photonics*, vol. 7, no. 11. American Chemical Society, pp. 2941–2951, Nov. 18, 2020. doi: 10.1021/acsphotonics.0c01245.

[119] W. K. H. Alhashemi, D. S. Zageer, and H. K. Risan, "Estimation the efficiency of sunlight UV on inactivation COVID-19 virus," *Egypt J Chem*, vol. 64, no. 7, pp. 3225–3234, Jul. 2021, doi: 10.21608/ejchem.2021.39728.2810.

[120] A. Montesinos-Castellanos, "Tec de Monterrey Air Purifying System Progress Fall 2020 ."